ChemComm

HIGHLIGHT

View Article Online
View Journal | View Issue

Cite this: *Chem. Commun.*, 2025, **61**, 11510

Advances in oxychalcogenide materials for hydrogen evolution photocatalysis in aqueous media†

Sandy Al Bacha, *[abc] Emma E. McCabe *[c] and Houria Kabbour *[ad]

The growing demand for sustainable energy solutions has led to significant research in photocatalytic water splitting, a promising approach for clean hydrogen production. Oxychalcogenide materials have emerged as a compelling class of photocatalysts due to their tunable electronic structures, various architectures, and favorable band edge positions for solar water splitting. This review provides a comprehensive analysis of recent advances in oxychalcogenide photocatalysts, emphasizing their structural diversity, composition–property relationships, and key design strategies. We highlight the impact of anion selection, cation contributions, charge carrier dynamics, and material stability on photocatalytic performance. Furthermore, we discuss innovative experimental approaches, such as surface modifications that have been employed to enhance activity. By consolidating existing knowledge and identifying critical parameters for optimization, this review aims to shed light on this class of photocatalysts and help guide the rational design of next-generation oxychalcogenide photocatalysts for efficient and scalable solar hydrogen production.

Received 14th March 2025,
Accepted 27th June 2025

DOI: 10.1039/d5cc01448d

rsc.li/chemcomm

[a] *Univ. Lille, CNRS, Centrale Lille, ENSCL, Univ. Artois, UMR 8181 – UCCS – Unité de Catalyse et Chimie du Solide, F-59000 Lille, France. E-mail: sandy.albacha@univ-lille.fr*
[b] *School of Physical Sciences, University of Kent, Canterbury, Kent CT2 7NH, UK*
[c] *Department of Physics, Durham University, Durham DH1 3LE, UK. E-mail: emma.mccabe@durham.ac.uk*
[d] *CNRS, Institut des Matériaux de Nantes Jean Rouxel – UMR6502, Nantes Université, F-44000 Nantes, France. E-mail: houria.kabbour@cnrs-imn.fr*

† Electronic supplementary information (ESI) available: Comparison tables of the structural and physical properties of oxysulfide, oxyselenide and oxytelluride materials. Estimated band edge positions using the empirical method of different oxychalcogenides. See DOI: **https://doi.org/10.1039/d5cc01448d**

Sandy Al Bacha

Sandy Al Bacha received her PhD in Chemistry of Materials in 2023 through a dual doctoral program between the University of Lille (France) and the University of Kent (UK), under the supervision of Dr Houria Kabbour and Dr Emma McCabe. Her first postdoctoral position at the CRISMAT laboratory in Caen focused on the development and optimization of advanced materials for thermoelectric applications. In March 2025, she rejoined the UCCS laboratory (CNRS–Lille) for a second postdoctoral fellowship, where she is currently investigating functional magnetic materials for data storage. Her research interests include the synthesis, characterization, and optimization of environmentally sustainable materials for energy conversion and storage applications.

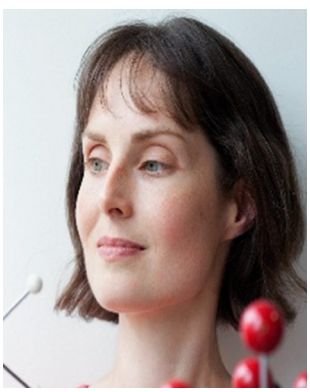

Emma E. McCabe

*Emma McCabe's research group focuses on structure–composition–property relationships in functional materials. The group design and synthesize new functional materials and investigate their structures and physical properties, such as magnetic, electronic and optical behaviour. We're interested in oxides (including perovskite-related materials) and mixed-anion materials (e.g. oxychalcogenides and oxyfluorides). Emma moved to the Department of Physics at Durham University in 2021 as Assistant Professor, then Associate Professor, after academic positions in chemistry at University of Kent. She is grateful to Max Alexander for use of the photo which was taken as part of the Illuminating Atoms exhibition (**https://www.maxalexander.com/galleries/illuminating-atoms-portraits/**) for the International Year of Crystallography.*

1. Introduction

Solar energy, the most abundant energy source[1–4] can be converted into chemical energy, for instance in the case of water-splitting photocatalysis,[5] other photocatalytic reactions[6] or photoelectrochemistry,[7] and into electrical energy by means of the photovoltaic effect. Photocatalysis has been developing for a long time, with early work on oxides like ZnO that introduced the concept of photo-reduction.[8] The observation that TiO_2 could catalyse the decomposition of organic materials (under UV light),[9] and then catalyse water splitting to give O_2 and H_2[10] has motivated research into new and efficient photocatalysts.[11–13] A schematic illustration of the photocatalytic reaction process indicating factors that may affect photocatalytic activity is presented in Fig. 1.

For photocatalysis, first the semiconductor has to be irradiated by incident photons of energy greater than or equal to the bandgap energy of the material. The absorption of photons will cause the excitation of electrons (e^-) from the valence band (VB) to the conduction band (CB) leaving a positive hole (h^+) in the valence band. The e^-/h^+ pairs will separate and migrate to the reaction sites on the surface of the material or recombine. In an ideal photocatalytic reaction, after the adsorption of the molecules (H_2O for water-splitting) involved in the reaction to be catalyzed, electrons and holes migrate to reaction sites and take part in reduction and oxidation reactions, respectively. In addition to the desired photocatalytic redox reactions, the e^-/h^+ pairs could recombine a short time after their separation, which is detrimental to the photocatalytic activity.[14,15] This recombination can result from various phenomena and was documented in various reports.[16,17] Some intrinsic properties of the photocatalysts such as built-in electrical field or high mobility charge carriers for instance are reported to enhance e^-/h^+ separation and rapid migration.[18] On the other hand,

Houria Kabbour

Houria Kabbour is a CNRS Research Director at the IMN (University of Nantes, France). Before joining IMN, she worked at the UCCS laboratory (University of Lille) and completed postdoctoral research at the California Institute of Technology and the Max Planck Institute for Solid State Research. Her research combines ab initio simulations and experimental approaches to design, synthesize, and characterize a wide range of functional materials. She investigates structure–properties relationships in diverse systems, including mixed-anion compounds, with a focus on magnetism, optical properties, and photocatalysis, and a particular interest in band gap engineering.

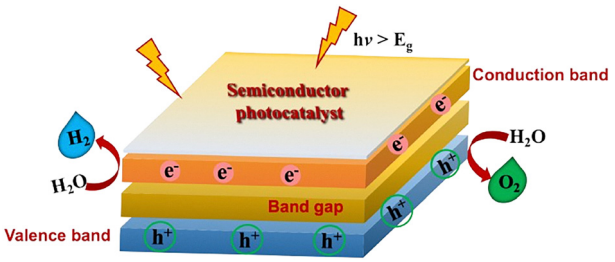

Fig. 1 Schematic illustration of the entire photocatalytic reaction process in a semiconductor photocatalyst.

approaches exploiting extrinsic factors, such as heterostructures and p–n junctions, can enhance this e^-/h^+ separation.

It is therefore, important to develop new and more sustainable strategies that can aid the future energy transition and maintain technological progress. In this context, fuel cells are one such example, as they use renewable sources (oxygen and hydrogen) to give electrical energy.[19] Since oxygen is readily available, the challenge is to produce the required hydrogen. To this purpose, solar photocatalytic water splitting is very attractive due to its simplicity: if the photocatalyst in appropriate conditions (solution, co-catalyst) is directly active using only sunlight to efficiently produce renewable hydrogen. Fig. 1 illustrates the process of the water splitting reaction in a typical semiconductor material on the conduction and the valence band level, with a suitable bandgap for the solar spectrum.[15,20]

However, carrying out solar photocatalytic water splitting imposes constraints on the semiconductor, such as the magnitude of the bandgap (between 1.23 and 3.10 eV, where 1.23 eV is the theoretical minimum bandgap, and 3.10 eV corresponds to the wavelength of the visible light ranging from 400 nm to 700 nm). Secondly, the conduction band potential must be more negative than the reduction potential of H_2O/H_2 (0 V) and the valence band potential must be more positive potential than the oxidation potential of O_2/H_2O (1.23 V),[21] to satisfy relations (1) and (2):

$$\text{Oxidation: } H_2O + 2h^+ \rightarrow 2H^+ + \frac{1}{2}O_2 \quad (1)$$

$$\text{Reduction: } 2H^+ + 2e^- \rightarrow H_2 \quad (2)$$

Oxychalcogenide photocatalytic materials gained considerable attention in recent years.[22,23] To understand their photocatalytic properties (and to design optimized oxychalcogenide photocatalysts), it is essential to understand their rich chemistry and structural diversity. Our review focuses on oxychalcogenide photocatalysts with bandgaps well-matched to the solar spectrum and with band edges of appropriate energies for photocatalytical water splitting. We explore compositions and structural features that play key roles in determining the photocatalytic activity of these oxychalcogenides. This understanding of structure–composition–property relationships allow us to propose some strategies to predict and design new oxychalcogenide photocatalysts.

2. Oxychalcogenides for photocatalysis

A mixed-anion compound is a material containing more than one anion in a single phase such as oxychalcogenides, oxypnictides,[24] oxyhydrides[25] and oxyhalides.[26] The coexistence of more than one anion type in the material is a promising strategy to control various properties, giving them a range of applications (photocatalytic activity[27–30] superconductivity,[31–33] magnetic,[34–36] non-linear optic (NLO),[37] battery material,[38] thermoelectricity[39] and photoluminescence[40]).

There are several reviews which highlight the importance of mixed-anion materials in general or for specific applications. Kageyama *et al.*[41] reviewed the great achievements and potential of mixed-anion materials, emphasizing some important factors in designing new materials. The different characters of the anions, such as charge, ionic radii, electronegativity and bonding character, can give rise to anion-order/disorder giving access to new structural types.[24] For example, oxynitrides often exhibit correlated disorder instead of a long-range one;[42] oxyarsenides show a long-range order of O^{2-} and As^{3-} anions (*e.g.* iron-based superconductors with insulating oxide layers and more delocalized (even superconducting) iron arsenide layers).[43,44]

Among mixed-anion materials, layered oxychalcogenides are a promising family that has gained more attention recently. Oxychalcogenides contain an oxide as well as a chalcogenide (sulfide/selenide/telluride) anion. These materials adopt a diversity of structure types and show a range of properties related to the ordering of the small oxide and the larger chalcogenide, likely due to their different sizes and bonding characters.[24]

Several excellent reviews have explored the structural chemistry of oxychalcogenides and their broader applications. Clarke *et al.*[24] examined the relationships between crystal structures and physical properties, while Orr *et al.*[45] focused on the structural diversity of rare-earth oxychalcogenides. Additional studies have highlighted their thermoelectric, optoelectronic, and infrared nonlinear optical properties.[46–48] Reviews on photocatalysis have also discussed mixed-anion materials, including oxychalcogenides, with key contributions from the Domen group[49,50] and others covering water-splitting, CO_2 reduction,[51] and heteroanionic photocatalysts.[52,53]

While these reviews provide valuable insights, our work offers a timely and dedicated focus on photocatalytic oxychalcogenides for solar water splitting. We consolidate recent advances, highlight critical structure–property relationships, and explore emerging strategies to enhance their photocatalytic performance. To our knowledge, no prior review has specifically addressed this class of materials with such depth in the context of solar-driven hydrogen production. In particular, we emphasize their potential for direct H_2 generation under sunlight, excluding more complex PEC systems and composite catalysts that combine sulfides and oxides.

2.1. Structures of oxychalcogenide materials

Oxychalcogenides, containing oxide anions as well as second larger and softer chalcogenide anion (*e.g.* S^{2-}, Se^{2-}, Te^{2-}), tend to stabilize lower transition metal oxidation states and lower coordination numbers, compared with oxides. As mentioned before, this family of materials show structural diversity, but they often adopt layered structures due to anion order that can lead to segregation of the different anions into different layers.[24] This layered arrangement of anions can depend on the relative electronegativities of the accompanying cations.[45] For instance, in the case of a significant difference in hardness/softness of cations, stronger bonds can be formed with either hard oxide or soft chalcogenide anions and so layered structures with a greater proportion of homoleptic (single anion) coordinations are favoured;[41] whilst in the case of similar hardness/softness of the cations, heteroleptic coordination (mixed anion) can be more favourable.[54]

These oxychalcogenides present some common structural features such as the building blocks that they contain (Fig. 2). For example, OLn_4 units in fluorite-like sheets, ribbons or chains (consisting of edge-linked units);[45,55,56] MQ_4 tetrahedra edge-linked into chains or antifluorite-like sheets[57] or square-based pyramid MQ_5 or MOQ_4 units for Bi, Sb with their $6s^2$ or $5s^2$ inert pairs.[58]

Having this layered aspect in most oxychalcogenides can give rise to a wide range of promising properties, due to the potential for chemical substitutions that can be done in both layers; such as highly anisotropic electronic structure and properties and high mobility semiconduction favored by the covalent aspect of the chalcogenide.[59] For example, layered LaOCuS[60] and BiCuOSe[61] are known as important thermoelectrics, due to the presence of the insulating oxide layers and the semiconducting copper chalcogenide layers (see Fig. 2).[46] As another example, $Ln_2O_2M_2OQ_2$, with M cations coordinated by both O^{2-} and Q^{2-} anions with long-range magnetic order, but electronically quite separated by the insulating $[Ln_2O_2]^{2+}$ layers.[62] These materials may have numerous properties such as magnetism,[63–65] thermoelectricity[48,66] IR-nonlinear optical materials,[47,67–70] second harmonic generation (SHG),[71–73] semiconductors,[74–76] photocatalysts[53] and piezoelectricity.[77]

2.2. Photocatalytic properties and band gap feature of oxychalcogenides

Several examples of oxychalcogenides for photocatalytic water splitting have been reported but to date there has not been a systematic exploration of their properties and features. A survey of the literature helped identify oxychalcogenides and their important characteristics (band gap, semiconduction type, cation choice, coordination environment, anion ratio and polarity); the band edge positions have also been estimated, which allowed the identification of some potential candidates for possible future characterizations (see ESI†). In the following section, the top materials with proven capacity to evolve H_2 and/or O_2 are discussed. These H_2(g) and/or O_2(g) evolution experiments have been reported for relatively few oxyselenides.

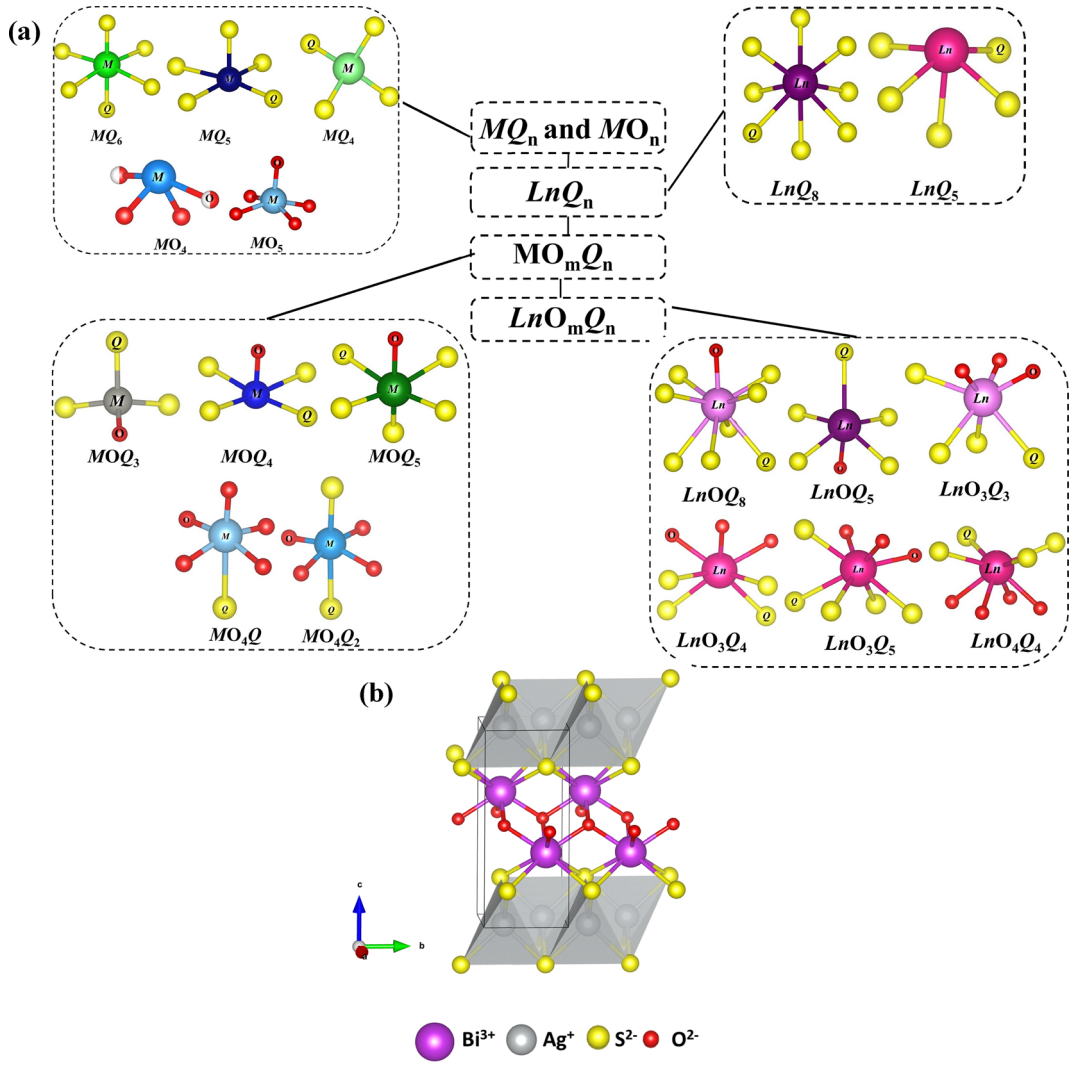

Fig. 2 (a) Schematic summarizing some coordination environments in oxychalcogenides. (b) Example of the ZrCuSiAs structure packing motifs from panel 1, adopted by BiCuOQ, BiAgOQ and LnFeAsO (as discussed in Section 2.2.8).

2.2.1. $Ln_2Ti_2S_2O_5$ (Ln = Y, Nd, Sm, Gd, Tb, Dy, Ho and Er) series. The series $Ln_2Ti_2S_2O_5$ (*Ln* = Y, lanthanide) adopt a tetragonal Ruddlesden–Popper crystal structure.[78,79] It is built from double-layers of corner-linked TiO_5 square-based pyramids separated by $[Ln_2S_2]^{2+}$ rocksalt slabs (Fig. 3) where this separation between the covalency of the sulfide layers and the ionicity of oxide layers results in an intermediate situation of strong interlayer connections. Optical band gaps of these phases were found to match the solar spectrum,[80] and under visible-light (λ = 440–650 nm) irradiation they demonstrated their capacity to evolve both O_2 and H_2 (Table 1).[81] Studies on $Sm_2Ti_2S_2O_5$ highlight the importance of the pH and the surface modification on the photocatalytic activity;[82] and the influence of the synthetic route with lower temperatures and reduced heating time to increase the photocatalytic activity, due to the formation of smaller particle sizes and, consequently, an increased surface area.[83] In addition, the n-type $Y_2Ti_2O_5S_2$[84] was the first to demonstrate a capacity to evolve both hydrogen and oxygen in a stoichiometric ratio, under visible irradiation.[85]

The fact of having suitable band gaps as well as a layered structure definitely contributed to the good activity demonstrated by this series. Another common factor is the presence of Ti 3d orbitals in the CBM; whilst for the VBM the lanthanide based phases have partially filled, highly localized, *Ln* 4f orbitals which are less effective in photoconductivity or photocatalysis and are usually ignored.[82] Finally some of these phases exhibited lower activities than others which could be related to the larger amounts of sulfur defects or the thermodynamically less favorable VB position.[81] More recently, Sc-doping of $Y_2Ti_2O_5S_2$ followed by an etching process to "clean" the surface, considerably increased the photocatalytic activity to 445 mmol h^{-1}, which is 3.4 times higher than that for the pristine compound. The authors attribute this enhancement to a decrease of the defect density with Sc doping.[86] In another article, $Y_2Ti_2O_5S_2$ nanosheets are synthesized by a flux-assisted solid-state reaction which exposed {101} and {001} facets that provides an anisotropic charge migration, which were found to be responsible for the reduction and oxidation of the water-

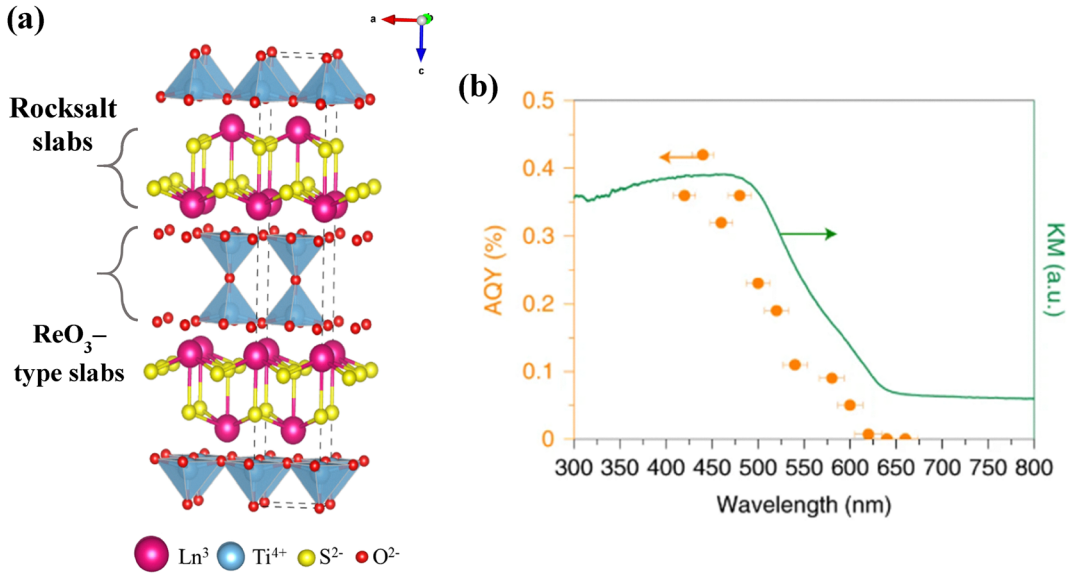

Fig. 3 (a) Structural representation of the Ruddlesden–Popper structure of the $Ln_2Ti_2S_2O_5$ series of *I4/mmm* symmetry; (b) shows apparent quantum yield (AQY) for overall water splitting and diffuse reflectance spectrum (DRS) measured for Cr_2O_3/Rh/IrO_2-modified $Y_2Ti_2O_5S_2$. Reproduced from ref. 85 with permission from Springer Nature.

splitting photocatalytic reaction, respectively. It is striking that selective photo-deposition of cocatalysts (on a particular facet) was possible and resulted in enhanced reactivity (H_2 production, (536 μmol h^{-1})).[84]

Several studies focused on this particular $Y_2Ti_2O_5S_2$ photocatalyst, each of them bringing innovative approaches to design the particles, the surface or the contact with the co-catalyst. Another study focused on the solid-state reaction mechanism and intermediate.[87] They thus found that from the traditional precursors Y_2O_3, TiO_2 and Y_2S_3, the three intermediate phases $Y_2Ti_2O_7$, Y_2O_2S and TiS_2 appear during the formation of the final oxysulfide. The formation of agglomerates involving $Y_2Ti_2O_7$ and Y_2O_2S which react with the third intermediate TiS_2 (carried by the sulfur vapor) was a critical step impacting the morphology of the crystallites. With this knowledge, the authors could reduce the particle size by increasing the heating rate which resulted in improved photocatalytic performances.

These advances on those compositions show that the intrinsic properties of the crystalline phases are as important as the morphology (particle size and surface design). In the case of *Ln* = Gd, outstanding results were reported with recent advances.[88] $Gd_2Ti_2O_5S_2$ with atomically ordered surfaces could be obtained using flux synthesis followed by acidic etching of the surface. The outstanding enhancement of the photocatalytic activity (3 mmol h^{-1} for H_2 production) is attributed to the crystals shape (platelet) combined with the surface design and optimized contact between the particles and a composite cocatalyst (Cr_2O_3/Pt/IrO_2).[89]

2.2.2. $SrZn_2S_2O$. The Zn-based oxysulfide $SrZn_2S_2O$ adopts a wurtzite-derived crystal structure consisting of double layers of corner-shared ZnS_3O tetrahedra separated by Sr^{2+} ions (Fig. 4).[90–92] $SrZn_2S_2O$ is an n-type semiconductor with a 3.86 eV direct band gap; the CB is dominated by the Zn 4s and 4p orbitals and the Sr 4d orbitals while the VB is mainly composed of O 2p and S 3p orbitals. $SrZn_2S_2O$ was capable on reducing and oxidizing water under UV-light irradiation, with a certain photocorrosive resistance.[92]

Compared to the $Ln_2Ti_2S_2O_5$ series discussed above, the O_2 evolution rate is similar but the H_2 evolution is slightly higher for $SrZn_2S_2O$ (Table 1). This indicates the advantage of having the Zn orbitals contributing to the CB compared to the Ti orbitals. $SrZn_2S_2O$ exhibits a structure with the presence of heteroleptic coordination environment (ZnS_3O) connected three dimensionally unlike the layered $Ln_2Ti_2S_2O_5$, which could also have an impact on the transport properties of the charge carriers.

2.2.3. $LnOInS_2$ (Ln = La, Ce, Pr). Yellow $LaOInS_2$ has a band gap of 2.73 eV and is a p-type semiconductor that adopts an orthorhombic structure.[93] Its crystal structure is composed of NaCl-type slabs made of InS_4 tetrahedra and InS_6, InS_5O octahedra, and $[LaO]^+$ fluorite-type ribbons alternating in different directions (Fig. 5a).[94] Under Xe lamp irradiation, the sample exhibited a reproducible photocatalytic activity, and showed H_2 evolution. On the other hand, using a metathesis reaction, the metastable layered polymorph of $LaOInS_2$ (also predicted in ref. 97), was synthesized. It has a direct band gap of ~2.64 eV, and it adopts a monoclinic structure consisting of alternately stacked $[InS_2]$ layers (rock-salt type) composed of InS_6 octahedra and oxide $[LaO]^+$ layers (PbO-type), with a split in the In sites (Fig. 5b). This polymorph was reported with higher rates of H_2 and O_2 evolution under visible light ($420 < \lambda < 800$ nm).[95]

Then again, $CeOInS_2$ and $PrOInS_2$ phases were found to be isostructural to the monoclinic layered $LaOInS_2$,[95] except that the indium in these phases is on-center unlike in $LaOInS_2$, which is off-center. They revealed direct band gaps of 2.41 and

Table 1 Photocatalytic activity of the oxysulfides discussed in this review. Rates are taken from the references or estimated from the reported gas evolution with time. Properties are given for photocatalysis (PC) except for $La_5Ti_2Cu_{1-x}Ag_xS_5O_7$ which was measured as a photocathode in a photoelectrochemical (PEC) system (unassisted)

Compounds		Cocatalysts		Rate of gas evolution (μmol h^{-1})	
		H_2 promotor	O_2 promotor	H_2	O_2
$Ln_2Ti_2S_2O_5$[81]	$Pr_2Ti_2S_2O_5$	Pt	—	0	0
	$Nd_2Ti_2S_2O_5$			4	3
	$Gd_2Ti_2S_2O_5$			24	21
	$Gd_2Ti_2O_5S_2$ with atomically ordered surfaces[88]			3000	
	$Tb_2Ti_2S_2O_5$			19	20
	$Dy_2Ti_2S_2O_5$			10	9
	$Ho_2Ti_2S_2O_5$			22	5
	$Er_2Ti_2S_2O_5$			21	1
$Y_2Ti_2S_2O_5$[85]		Cr_2O_3/Rh/IrO_2		~50	~25
$Y_2Ti_2S_2O_5$ nanosheets[84]		Pt	IrO_2	536	
Sc-doped $Y_2Ti_2O_5S_2$[120]		Rh		445	
$Sm_2Ti_2S_2O_5$[82,83]		Pt	IrO_2	22	22
$SrZn_2S_2O$[92]		Pt	IrO_2	67.8	26.9
$LaInOS_2$	α-$LaInOS_2$[94]	Pt	—	5.1	—
	Layered-$LaInOS_2$[95]	Pt	IrO_2	~25	~6
$AInOS_2$[96]	$CeInOS_2$	Pt	—	<2.5	—
	$PrInOS_2$	Pt	—	<2.5	—
$La_5In_3S_9O_3$[100]		Pt	IrO_2	~50	~12
La_3GaS_5O[103]		$RuCl_3{\cdot}3H_2O$	IrO_2	80.7	~12
$La_3NbS_2O_5$[112]		Pt (1 wt%)	—	3–11	—
$La_5Ti_2MS_5O_7$[105,106]	$La_5Ti_2CuS_5O_7$	Pt	IrO_2	110	24
	$La_5Ti_2AgS_5O_7$	Pt	IrO_2	220	12
$La_5Ti_2Cu_{1-x}Ag_xS_5O_7$[121]		Pt	—	~32	—
Ga doped – $La_5Ti_2Cu_{0.9}Ag_{0.1}O_7S_5$[111]		Rh (imp + ph)		464 μmol H_2 during the first hour	
$La_5Ti_2Cu(S_{1-x}Se_x)_5O_7$[110]		Pt/NiS			
BiOAgS[113]		Ru	—	~10	—
$ZnO_{0.6}S_{0.4}$[115]					
$InMnO_{3-x}S_x$[122]				158 (sacrificial S^{2-}/SO_3^{2-})	649 (with specific $AgNO_3$ sacrificial agent)
Defect-$(Bi,Ce)_2(O,S)_{3-x}$ nanorods[118]				526.5	
$Sn_2Nb_2O_{7-x}S_x$ (up to $x = 0.6$)[114]				6	
$Zn(Zn,Ni,In)_2(O,S)_{4-x}$[117]				1700	

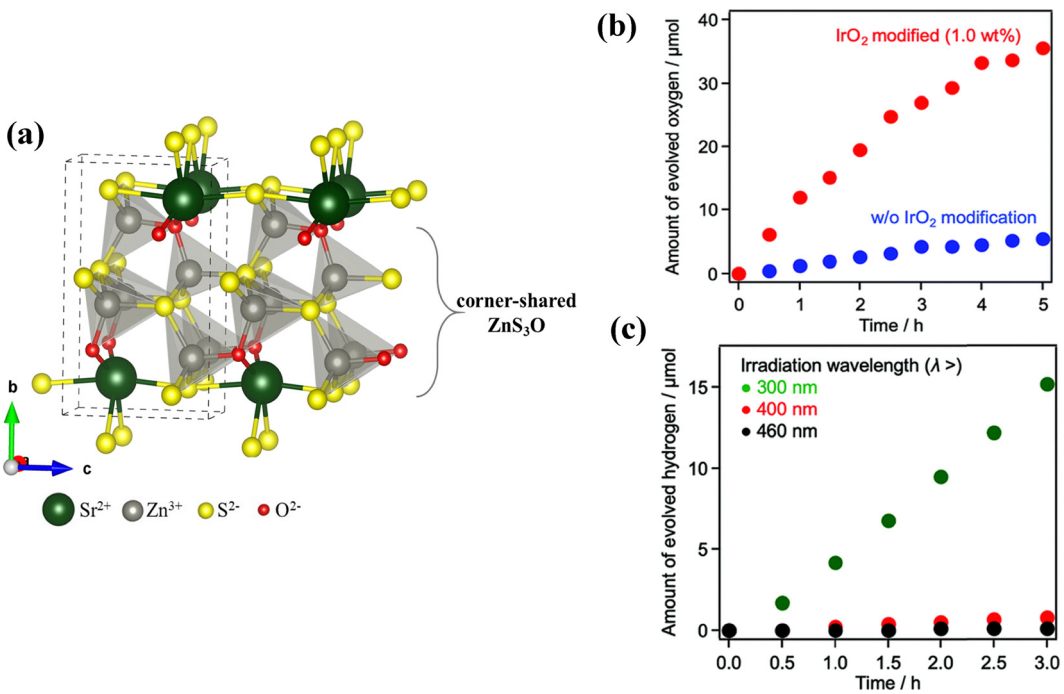

Fig. 4 (a) Structural representation of $SrZn_2S_2O$ oxysulfide of $Pmn2_1$ symmetry; (b) oxygen evolution for $SrZn_2S_2O$ and (c) hydrogen evolution for Pt/$SrZn_2S_2O$. Reproduced from ref. 92 with permission from the Royal Society of Chemistry.

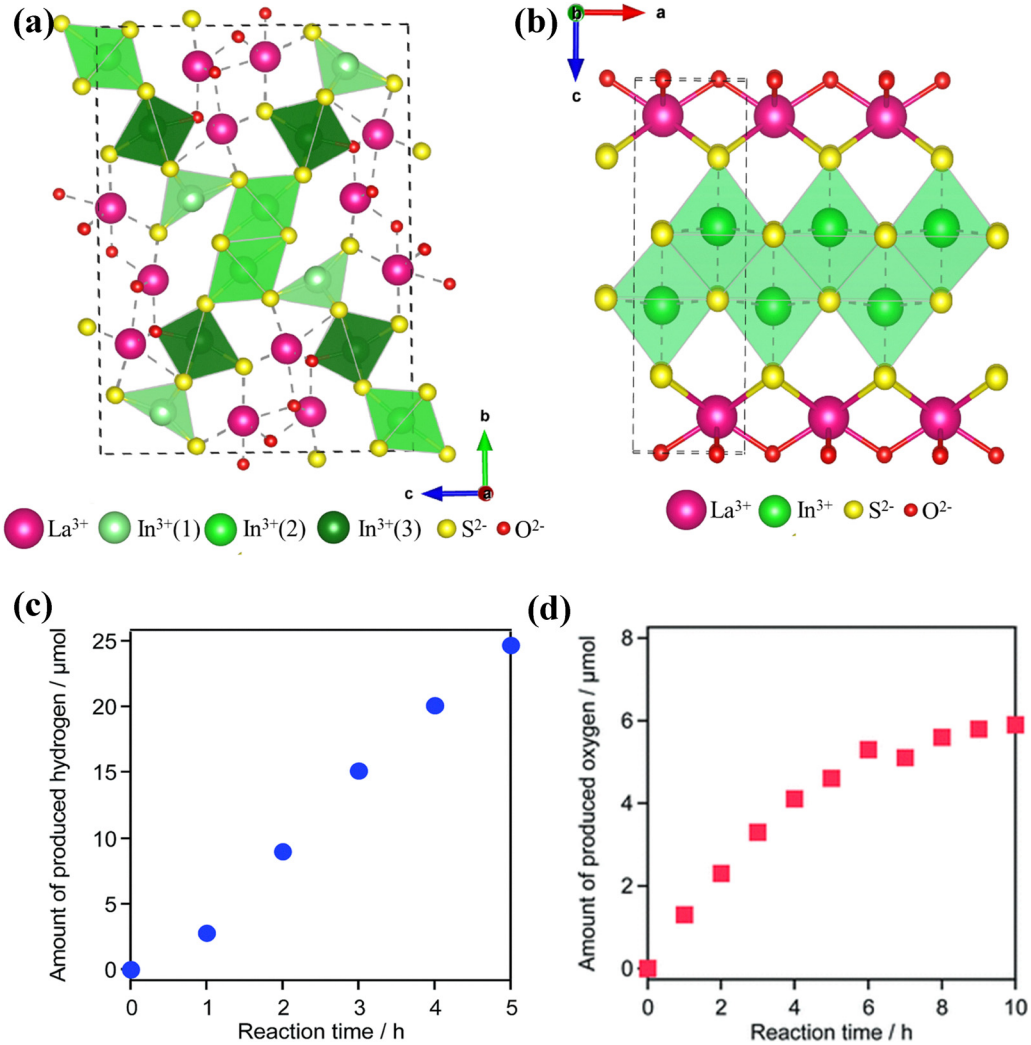

Fig. 5 Structural representation of $LaOInS_2$ material with (a) alpha model of *Pbcm* symmetry and (b) metastable layered model of $P2_1/m$ symmetry; below, the water splitting properties of the metastable layered phase of $LaOInS_2$ are shown including (c) H_2(g) evolution for 0.75 wt% Pt/$LaOInS_2$ and (d) O_2(g) evolution for 0.5 wt% IrO_2/$LaOInS_2$. Reproduced from ref. 95 with permission from the Royal Society of Chemistry.

2.43 eV, respectively. Compared to $LaOInS_2$, these phases showed reduced H_2 evolution (it decreased by 10% under visible light).[96]

The CBM in the La-based phases is mainly composed of In 5s/5p orbitals, whilst O 2p and S 3p contribute most to the VBM. The In states seem beneficial in that they contribute to the higher dispersion of the CBM (that should be associated with lower effective masses of the charge carriers and thus higher mobilities) and thus increase the capacity to evolve H_2. However, the layered polymorph exhibited higher rates, probably related to the structure dimensionality (compared to the α-$LaOInS_2$): the layered character gives efficient separation of the charge carriers and helps to avoid their recombination, and thus benefits to the photocatalytic reaction. However, measurements with the same conditions are needed to evaluate accurately the difference in H_2 release rate for the two polymorphs.

As for $CeOInS_2$ and $PrOInS_2$ phases, the presence of the on-center indium decreased the hybridization of the In 5p–S 3p orbitals, which resulted in an increase in the energy difference of these hybridized orbitals, slightly shifting the optical absorption edge of these phases.[96] Even though the 4f orbitals of *Ln* are negligible when highly localized, it seems that their presence might increase the electron–hole recombination rates.[97,98]

2.2.4. $La_5In_3S_9O_3$. The structure of $La_5In_3S_9O_3$ consists of fluorite-type ribbons of lanthanide ions alternating with rock-salt InS layers to form 2D $La_5In_3S_6O_3$ layers in a zigzag pattern (Fig. 6).[93] In^{3+} cations are only coordinated by sulfur, while La^{3+} ions are coordinated by both oxide and sulfide ions (similar to other La–In based compounds[99]). The optical band gap of the yellow powder was 2.60 eV, slightly smaller than that of $LaInS_2O$ (2.73 eV), probably due to the increased sulfur coordination in $La_5In_3S_9O_3$ decreasing the band gap.[93] Even though a pure polycrystalline phase was not obtained for the p-type semiconductor $La_5In_3S_9O_3$, it was able to reduce and oxidize water under visible irradiation.[100] A stable H_2 evolution occurred,

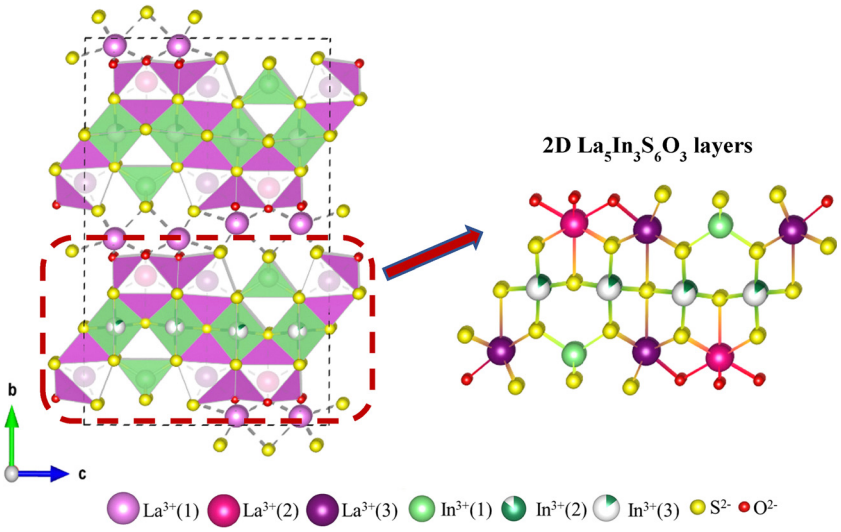

Fig. 6 Structural representation of $La_5In_3S_9O_3$ oxysulfide (*Pbcm* symmetry) with the 2D $La_5In_3S_6O_3$ layers consisting of two building blocks: rock-salt layers formed by both indium and lanthanum and fluorite-type ribbons formed by lanthanum atoms; alternating regularly along *b*.

unlike the O_2 evolution where it decreased over time (due to the deposition of metallic silver).

Similar to the $LnOInS_2$ (Ln = La, Ce, Pr) series, the presence of the In 5s–5p orbitals contributes to the higher H_2 evolution efficiency.[82] This is similar to $SrZn_2S_2O$, with the presence of the Zn 4s–4p orbitals contributing to the enhanced H_2 evolution.

2.2.5. La–Ga based oxysulfides ($LaGaS_2O$ and La_3GaS_5O). $LaGaS_2O$ adopts an orthorhombic KVO_3-type structure consisting of layers of corner-shared distorted GaO_2S_2 tetrahedra sharing oxygen with La^{3+} cations (Fig. 7a).[101] La_3GaS_5O adopts an orthorhombic shear type structure consisting of corner-shared GaS_4 tetrahedra layers and a second layer of $(La_2O)_n$ formed by edge sharing LaS_2, LaS_2O and $LaSO_2$, both parallel to the *b* direction (Fig. 7b).[102]

$LaGaS_2O$ demonstrated a n-type semiconduction with an indirect band gap of 3 eV whilst La_3GaS_5O exhibited a n-type semiconduction with a direct band gap of 2.3 eV. The CBM level is similar in both phases, whereas the VBM in La_3GaS_5O is higher than $LaGaS_2O$, due to the higher sulfur content. Both phases were found to be potential photocatalysts but only La_3GaS_5O was tested for water reduction and oxidation reactions under visible light, whilst $LaGaS_2O$ produced anodic photocurrent under ultraviolet light.[103] The comparison of these phases highlights the importance of the chalcogen ratio in narrowing the band gaps.

2.2.6. $La_5Ti_2MS_5O_7$ (M = Cu, Ag) systems. $La_5Ti_2MS_5O_7$ (*M* = Cu, Ag) oxysulfides adopt an orthorhombic structure that is not layered but rather presents condensed fragments of layers that form a building unit repeating periodically along the *b* direction (Fig. 8). It consists of: (i) rock-salt-type fragment containing CuS_4 tetrahedra, (ii) perovskite building block made of double chains of corner-sharing Ti-centered octahedra (TiO_4S_2 or TiO_5S). The orange-yellow powder revealed an optical band gap of 2.02 and 2.17 eV for Cu and Ag phases, respectively.[104] Preliminary photoelectrochemical measurements revealed p-type semiconduction and a photocatalytic activity under visible light;[105] with higher rates occurring when loaded with convenient amount of cocatalysts.[106]

Various synthesis methods to produce the photocathode $La_5Ti_2CuS_5O_7$ were investigated to further enhance its photocatalytic properties.[107,108] The electronic band structures of these phases were found to be suitable for charge separation and revealed a CBM consisting of Ti 3d orbitals whilst the VBM was formed by hybridized Cu 3d and S 3p orbitals in $La_5Ti_2CuS_5O_7$, rather than just S 3p orbitals in $La_5Ti_2AgS_5O_7$, responsible for the longer absorption edge wavelength.[106] The study of these materials highlights the importance of having disassociated paths for accelerating the charge separation while inhibiting the recombination process.[109]

Substituted phases were also investigated for their photocatalytic properties in this system such as $La_5Ti_2Cu(S_{1-x}Se_x)_5O_7$ photocatalysts and their hydrogen evolution activity. The authors show that performances decrease with Se content due to excessive crystals growth which can be limited by controlling the calcination temperature.[110]

On the other hand, the experimental study of Ga doped-$La_5Ti_2Cu_{0.9}Ag_{0.1}O_7S_5$ synthesized using thermal sulfidation show that post annealing in sulfur vapor improved its properties (H_2 production of 464 μmol h^{-1}) by reducing the defect concentration at the surface and achieving smaller particle sizes. The best samples reached H_2 production of 400 μmol after 4 hours in Na_2S–Na_2SO_3 solution and with Rh as cocatalyst.[111]

2.2.7. $La_3NbS_2O_5$. For the oxysulfide $La_3NbS_2O_5$ (Fig. 9), the preparation was carried out by sulfurization (with H_2S) of a reactive oxide precursor La_3NbO_7; the longer the treatment, the greater the particle size which decreased the BET surface area. The H_2 production was measured (3–11 μmol h^{-1} with Pt as co-catalyst).[112]

2.2.8. Oxysulfide photocatalysts with ZrSiCuAs structural type. BiOAgS, which crystallizes in the ZrSiCuAs structure type, has been reported to be active for water-splitting. It exhibits

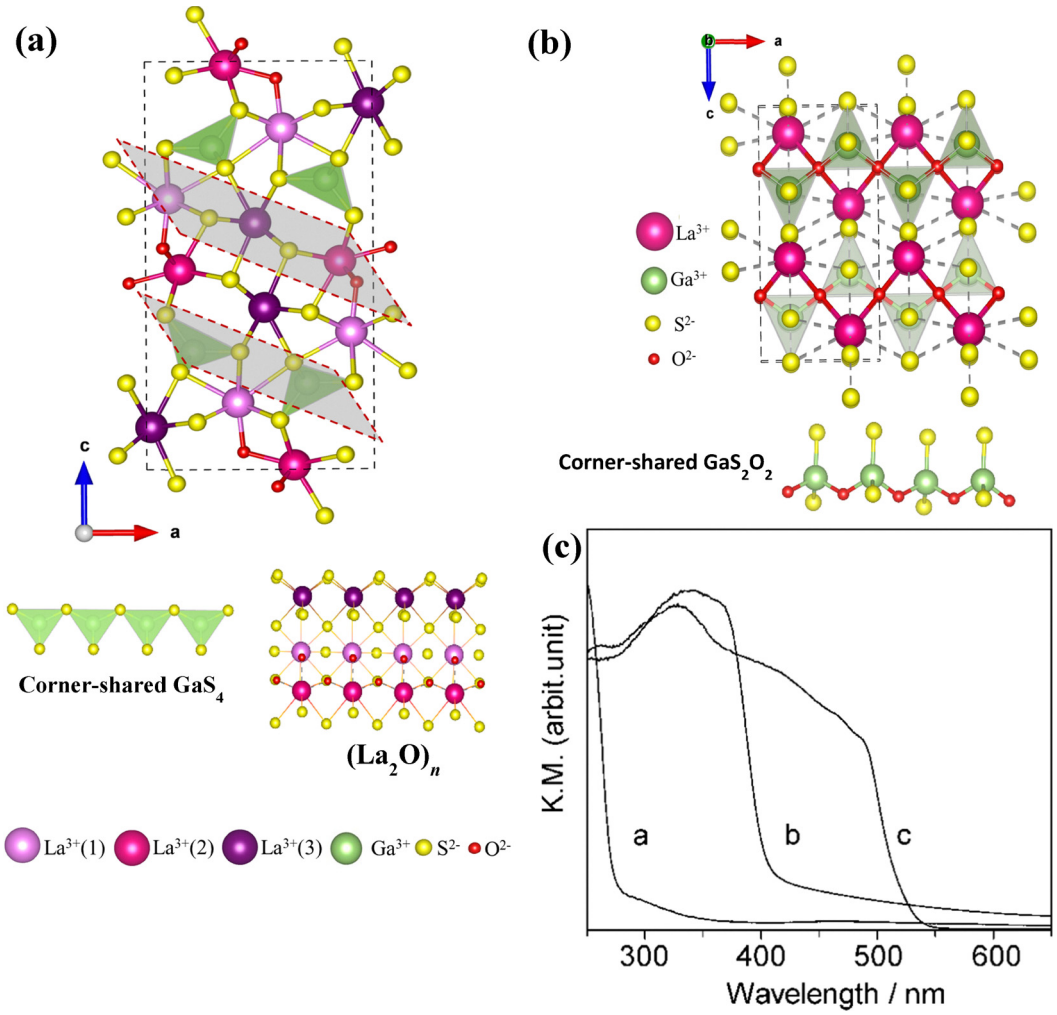

Fig. 7 Structural representation of (a) La_3GaS_5O (*Pnma* symmetry) and (b) $LaGaS_2O$ (*Pmca* symmetry) and, highlighting the different layers between the two compounds; (c) shows diffuse reflectance data for (a) $LaGaO_3$, (b) $LaGaS_2O$ and (c) La_3GaS_5O. Reprinted (adapted) with permission from [*J. Phys. Chem. C*, 2008, **112**(31), 11978–11984]. Copyright 2008 American Chemical Society.

(BiO) fluorite layers stacked with deficient ($Ag_{1-x}S$) antifluorite layers, (see Fig. 2b). With its more ionic character than the well-known BiOCuS, it has a larger dielectric constant and is interesting for photoconversion (efficient screening of photo-generated charges). It exhibits low effective masses, a band gap of 1.5 eV, a p-type character and the authors showed its ability to evolve H_2 with preliminary measurements using ruthenium (as co-catalyst photo-deposited in a Na_2S–Na_2SO_3 solution), which is not observed for BiOCuS.[113]

2.2.9. A pyrochlore oxysulfide. The Sn^{2+}-based pyrochlore oxysulfide $Sn_2Nb_2O_{7-x}S_x$ (up to x = 0.6) (Fig. 10a) is derived from the pyrochlore oxide $Sr_2Nb_2O_7$ and is synthesized using solid state reaction in an evacuated sealed quartz tube. The authors could incorporate different O : S ratios up to x = 0.6 and observe a gradual decrease of the band gap with increasing sulfur content (Fig. 10c). The resulting narrow band gap materials are active for water-splitting photocatalysis under visible light with highest amount of H_2 obtained for x = 0.4 (6 μmol h^{-1}), Fig. 10b.[114]

2.2.10. Other oxysulfide types. Simple compounds such as mono-cationic oxides substituted with sulfur also offer great potential to design functional oxysulfides. This is the case of $ZnO_{0.6}S_{0.4}$ which was reported with concomitant photocatalytic H_2 production (147.5 μmol h^{-1}) and pollutant degradation in a Na_2S–Na_2SO_3 solution, the two processes acting synergistically to reinforce the reactivity. Indeed, electron-donating intermediates (identified from FTIR) induced by the photodegradation reaction are suggested to boost the H_2 production at a particular concentration of the dye. This later approach constitutes another innovative experiment design to complement the intrinsic features of the oxysulfide matrix, in order to enhance reactivity.[115] Ni-doped Zn(O,S) oxysulfides were also reported based on simple low temperature methods.[116] In the later study, the highest H_2 production (14 800 μmol g^{-1} h^{-1}) was reached in a 50% ethanol solution.

The spinel compound $Zn(Zn,Ni,In)_2(O,S)_{4-x}$ is one of the few oxysulfides reported for this structure-type which have a complex non-stoichiometric composition. The later feature and

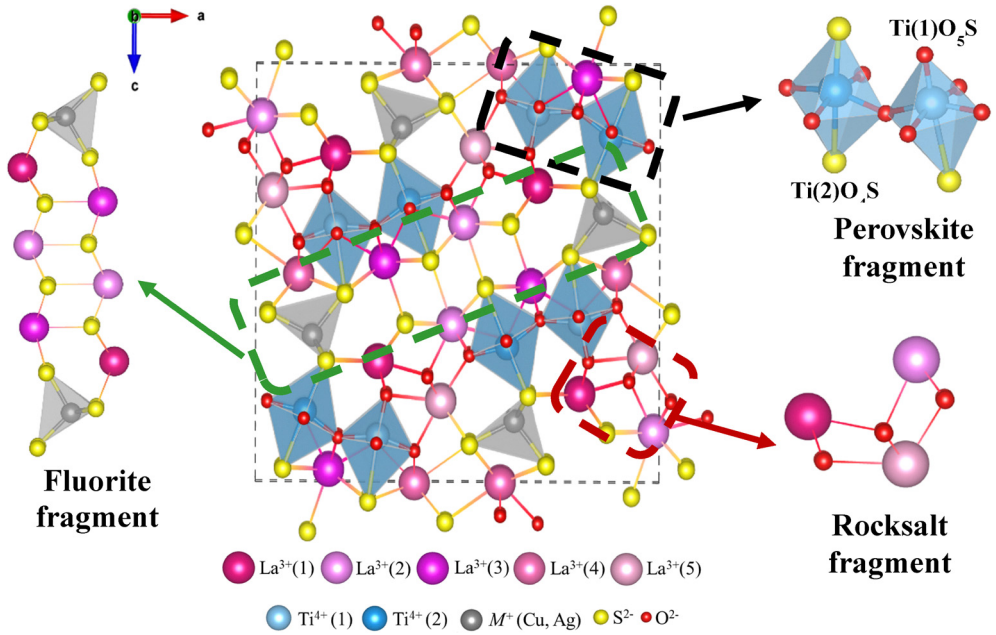

Fig. 8 Structural representation of (a) $La_5Ti_2MS_5O_7$, (M = Cu, Ag) oxysulfides (*Pnma* symmetry) highlighting the different building blocks within the structure.

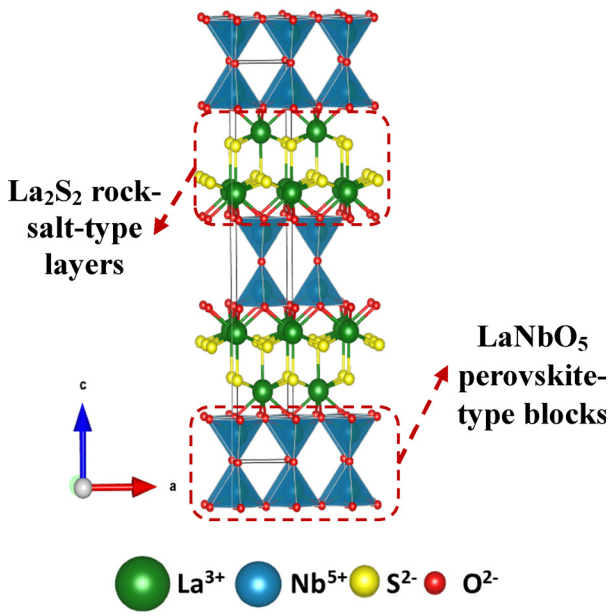

Fig. 9 Structural representation of the Ruddlesden–Popper-related phase $La_3NbS_2O_5$ oxysulfide (*I*4*mmm* symmetry), neglecting disorder in O(2) site positions.

its associated defect states are believed to enhance the photocatalytic H_2 production under visible light, which has been reported as 1700 μmol g^{-1} h^{-1}.[117]

Finally, we can cite another complex material which was designed with simple binary parent compounds as models. It is the defect-$(Bi,Ce)_2(O,S)_{3-x}$ nanorods in which the control of oxygen vacancies led to rapid electron transport resulting in excellent photocatalytic properties (526.5 μmol h^{-1} for H_2).[118]

2.3. Summary of composition and structural features observed in photocatalytic oxychalcogenides

A range of factors can affect the outcome of the overall water splitting photocatalytic reaction: (i) morphology and microstructure such as defects and crystallinity (intrinsic features) and (ii) pH, temperature, concentration of the catalyst, type and amount of cocatalyst loading, incident light intensity (extrinsic features). The focus of this survey is to compare the structural (connectivity, polarity) and electronic (band gap magnitude and nature, density of states, charge carriers' behaviour) properties, which allowed us to identify some key features/characteristics (including structural and relating to connectivity, and compositional) that contribute to the good activity of these materials:

- Higher sulfur content can increase the VBM position (as illustrated by comparison of $LaGaS_2O$ with La_3GaS_5O, Section 2.2.5), more suitable for the oxygen evolution but this can create larger amounts of defects within the structure which can be a disadvantage for photocatalytic activity.
- The charge carriers' behaviour is a very important factor and having a structure that enables disassociated paths for the photoexcited electrons and holes enhances their separation and decreases the rate of their recombination, as discussed for $La_5Ti_2MS_5O_7$ (Section 2.2.6).
- Cations with highly localized 4f orbitals, such as Sm, are less effective in photocatalysis and their contribution is usually ignored. On the other hand, cations with less localized 4f orbitals, such as Ce or Pr, can potentially increase the recombination rate of the photoexcited charges therefore decrease the photocatalytic activity, as suggested for the $LnOInS_2$ series (Section 2.2.3).
- Highly dispersed conduction and valence bands are definitely an asset for better H_2 and O_2 evolution, respectively. Examples include the presence of *ns*–*n*p orbitals (in In or Zn containing

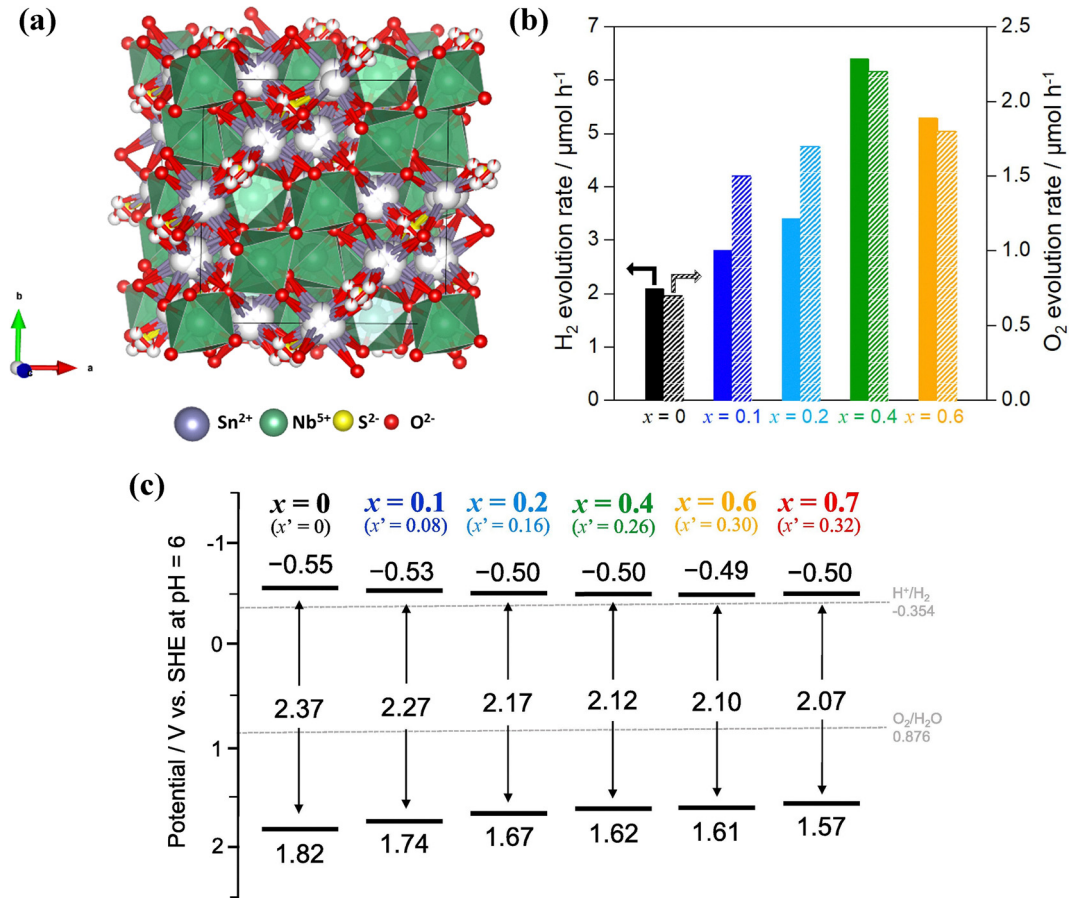

Fig. 10 (a) Structural representation of the Sn^{2+}-based pyrochlore oxysulfide $Sn_2Nb_2O_{7-x}S_x$ (x = 0.23) ($Sn_{2.55}Nb_{1.95}O_{6.26}S_{0.23}$); where some anion-order occurs and the sulfide anion is shown preferentially occupying the larger 8b site in the cubic pyrochlore structure. Panel (b) shows H_2(g) and O_2(g) evolution over $Sn_2Nb_2O_{7-x}S_x$ from water with an electron donor and acceptor, respectively, and (c) shows band edge positions for $Sn_2Nb_2O_{7-x}S_x$. Reprinted from J. Photochem. Photobiol., A, **444**, 114895, Copyright (2023) with permission from Elsevier.

materials) highly hybridizing in the CBM, or the addition presence of 3d orbitals (in Y or Cu containing materials) strongly hybridizing with the S 3p and O 2p orbitals gives a better VBM position.

• A greater energy difference between cation and anion orbitals can reduce their hybridization, which in turn may lower photocatalytic activity. This effect can be influenced by structural factors, such as cation displacement, either on or off-center, particularly in the case of ns^2 cations. The second-order Jahn–Teller effect plays a key role here, as the stereochemical activity of the lone pair can distort the local coordination environment, altering orbital overlap and hybridization strength.[119] This strategy has not yet been fully explored and is discussed below (Section 3.1.2).

3. Proposed design strategy for active oxychalcogenide photocatalysts

3.1. Key structural and electronic structure features of oxychalcogenides for photocatalysis from experimental and theoretical work

3.1.1. Choice of anion. Mixed-anion materials allow some tuning of the bandgap by choice of anion, particularly relevant for solar photocatalysis. For example, introducing softer anions (chalcogenides) in an oxide sublattice to give mixed-anion oxychalcogenides can introduce higher energy states at the top of the valence band, reducing the bandgap. This strategy is effective to tune the bandgap and meet the requirements of water splitting under visible light and give effective photocatalysis.[123,124] For example, antimony oxides such as α-Sb_2O_3 present large bandgaps (3.38 eV),[125] whilst antimony chalcogenides such as Sb_2S_3 and Sb_2Se_3 present narrower bandgaps (2.16 and 1.66 eV for S and Se, respectively).[126] Therefore, a mix of both oxide and sulfide can give a moderate bandgap, *e.g.* Sn^{2+}-based pyrochlore oxysulfide $Sn_2Nb_2O_{7-x}S_x$[114] suitable for the solar spectrum such as $Sr_6Cd_2Sb_6O_7S_{10}$ and $Sr_6Cd_2Sb_6O_7Se_{10}$ (1.89 and 1.55 eV for S and Se, respectively).[71,73]

3.1.2. Choice of cation. Cation choice for photocatalysts can be a key feature. Lone pair cations for example (Bi^{3+}, Sb^{3+}, Sn^{2+}) can induce oriented dipoles[127] which favour lower-symmetry coordination environments.[128] The relative energy of the ns^2 lone pair electrons to the anion p orbitals can determine the energy of states at the top of the valence band which are key to explaining the optical response of these materials.[129,130] This key feature was found to be effective in designing photocatalytic and photovoltaic materials.[131–133] Metal cations in higher

oxidation states are not always compatible with the oxychalcogenide redox chemistry (there's increased risk of the metal cation oxidizing the chalcogenide).[134] Then again, cations with slightly localized nf orbitals can increase the recombination rates[96] and cations with the presence of nd orbitals or highly hybridizing ns–np orbitals can increase the dispersion of the valence and conduction bands, respectively, giving more efficient charge carrier transport.[100,122]

3.1.3. Connectivity. The impact of the connectivity of the photoactive units on the photocatalytic outcome is still under investigated but it is certain that having a layered structure is advantageous, especially for the transport properties of the photoexcited charges.[135] The connectivity of the different building blocks within the structure can give different pathways for the electrons and the holes which can diminish their recombination during the photocatalytic reaction. The presence of this feature in most oxychalcogenides can promote the fast mobility which favours the charge migration to the surface of the photocatalyst to participate in the reaction, whilst slow mobility is more prone to result in charge recombination. Consequently, having distinct pathways for the mobility of charge carriers could be useful for the separation of e^- and h^+, reduction of the e^- and h^+ recombination rate, and improvement of the photocatalytic activity.[136–139] Besides this general tendency, high H_2 photocatalytic production was also demonstrated in a few non-layered oxysulfides, as discussed above, such as the spinel compound $Zn(Zn,Ni,In)_2(O,S)_{4-x}$. This might also offer structural types less encountered for oxysulfides to design photocatalysts, and their better comprehension would be also of great interest.

Overall, this issue should be possible to address more accurately using specific theoretical calculations. For instance, in a recent study, the electron and hole transport properties could be investigated based on real-time time-dependent density functional theory (TDDFT) and nonadiabatic molecular dynamics (NAMD).[140] Based on the excited-state dynamics, $Y_2Ti_2O_5S_2$ was found to exhibit a carrier lifetime much longer than that reported for lead-halide Perovskites. The authors identify a key factor underlying the high photocatalytic activity of this oxysulfide: the presence of distinct vibrational modes within different structural sublayers that contribute to nonadiabatic coupling (NAC). NAC describes how electronic transitions are influenced by atomic vibrations, and in this case, it facilitates efficient and spatially separated transport paths for electrons and holes, thereby enhancing charge separation and suppressing recombination (Fig. 11).

3.1.4. Stability with respect to oxidation. Another key feature is the materials' stability in water/aqueous solution, which needs to be adequate for successful photocatalytic applications. As mentioned earlier, oxides have demonstrated good stability as photocatalysts but on the other hand, chalcogenides haven't, and can suffer from sulfide and/or cation oxidation.[134] Oxychalcogenides offer a moderate stability (better than the sulfide/selenides), where the introduction of the O 2p orbitals gives more stability to the system.[141] Future work should focus on optimizing the morphology of oxychalcogenides to enhance their stability in aqueous environments. Strategies such as nanostructuring, surface modification, and heterostructure formation could help mitigate degradation while maintaining photocatalytic efficiency. Additionally, tailoring electrolyte compositions, such as adjusting pH levels or incorporating stabilizing agents may further improve the long-term durability of these materials. These strategies will be key to overcoming degradation challenges and ensuring long-term photocatalytic performance.[142]

3.1.5. Polarity. Lastly, polarity in heterogeneous photocatalysts has been shown to enhance charge-carrier separation, resulting in superior efficiency for example for photocatalytic water splitting.[143] Having polar distortions can also increase the bandgaps, although this increase is minimal in the case of oxides ($SrTiO_3$ for example[144]), it is much larger in the case oxysulfides, and because of the lower electronegativity of the sulfide.[145] This hypothesis was further investigated by Vonrüti and Aschauer[146] using DFT to study the suitability of polar $AB(O_xS_{1-x})_3$ perovskites for photocatalytic water splitting. It was found that the presence of polar distortions, induced by epitaxial strain (for oxynitrides[147]) or substitution of sulfur by oxygen (for oxysulfides) can be a promising route to suppress the recombination phenomena of the charge carriers. This is due to the out-of-plane spontaneous polarization arising from epitaxial strain on the anion order within the structure, which creates an electric field gradient across the active cation or even the entire material. This field is thought to enhance electron–hole separation, reducing recombination and thereby improving photocatalytic efficiency. It is important to distinguish between the polarity of the overall crystal structure and the local polarity of the cation coordination environments. While global polar distortions can give rise to a macroscopic electric field that enhances charge separation, local polarity in heteroleptic coordination environments (where a cation is coordinated by two types of anions) may also play a crucial role. Such local distortions can modify the electronic structure at the active site, further improving charge separation and transport. In particular, materials with heteroleptic units, which are often intrinsically polar, may exhibit enhanced electron–hole separation, which is crucial for improved photocatalytic activity.[146]

3.2. Design strategy for oxychalcogenide photocatalysts

Based on the key features in oxychalcogenide photocatalysts discussed in the previous section, we will therefore propose a potential design strategy that could be serve as a useful tool for designing new efficient oxychalcogenide materials for photocatalysis specifically, solar water splitting photocatalysis. A schematic diagram of a potential design strategy for efficient oxychalcogenide materials is presented in Fig. 12.

First, the nature of the bandgap (direct or indirect), the semiconduction type (n or p-type) are not of great influence on the properties of the photocatalysts as both types were exhibited by the materials discussed in Section 2.2. However, ensuring that the oxychalcogenide has a band gap well-matched in magnitude to the solar spectrum is essential. This can be achieved by selecting a softer chalcogenide anion Q^{2-} and by tuning the $O:Q$ ratio. Additionally, incorporating chalcogenides

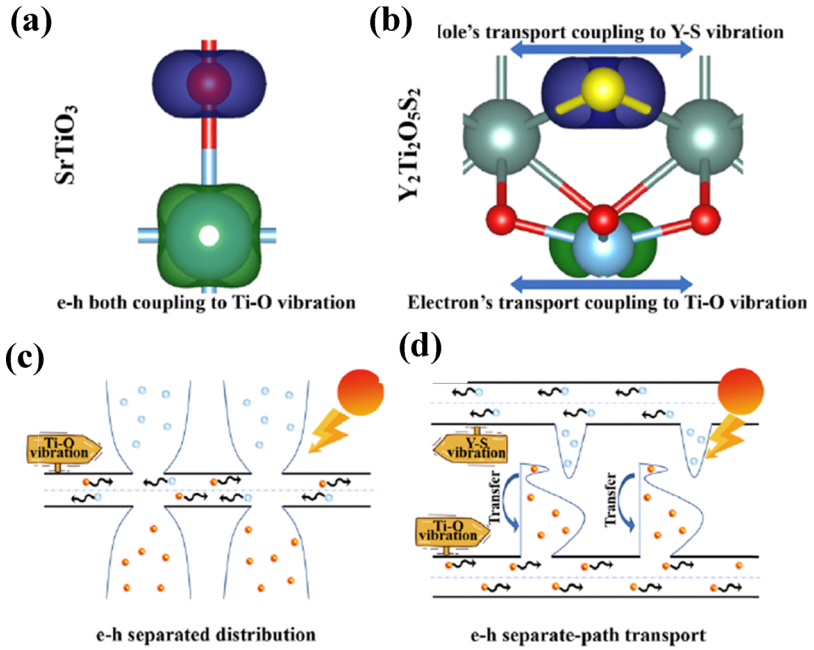

Fig. 11 The charge densities of the VBM (in purple) and CBM (in green) in (a) $SrTiO_3$ and (b) $Y_2Ti_2O_5S_2$. Electrons and holes in bad edges are distributed around metallic and non-metallic atoms, respectively. In $SrTiO_3$, the e–h only couple to Ti–O bonds, whereas the e–h couple to Ti–O and Y–S bonds in $Y_2Ti_2O_5S_2$, respectively. (c) The schematic drawing of the e–h separated distribution with a crowded transport channel in a crystal containing less than four elements, such as in $SrTiO_3$ with relatively weak carrier transport ability. (d) The schematic drawing of e–h separate-path transport in $Y_2Ti_2O_5S_2$. The holes in $Y_2Ti_2O_5S_2$ mainly diffuse within the $[Y_2S_2]^{2+}$ layer, and electrons mainly move within the $[Ti_2O_5]^{2-}$ layer. The blue and red balls represent the distribution of holes and electrons in real space, respectively. Reproduced from ref. 140 with permission from PCCP Owner Societies.

can increase bandgaps due to enhanced covalency, resulting from their lower electronegativity compared to oxygen.[145]

The structure and its connectivity are important for the transport properties of the photoexcited charges. Different pathways for the electrons and the holes help reduce the probability of recombination and this is often observed for layered or segmented structures. The band structure gives insight to the electronic properties of the material, in particular the effective masses of the charge carriers which describes their mobilities: higher dispersion of the bands close to the Fermi level indicate lower effective masses and hence higher carrier mobility and therefore enhanced transfer process. Recently, Li *et al.*[148] reported that the recombination of photogenerated electrons and holes can be much faster than the transport from bulk to the surface reactive site and the catalytic reaction. Thus, fast mobility favours the charge migration to the surface of the photocatalyst to participate in the reaction, whilst slow mobility is more prone to result in charge recombination. Therefore, having a large mobility difference could be useful for the separation of e^- and h^+, reduction of the e^- and h^+ recombination rate, and improvement of the photocatalytic activity.

Cation choice is another important feature due to the contributions of their corresponding orbitals to the band edges; this can therefore tune the band gap as well as the charge carriers' transport properties. Lastly, the polarity, is not widely studied as a design feature in photocatalysis, but it could enhance a catalyst's performance by improving charge carrier separation, as seen in ferroelectrics such as $AB(O_xS_{1-x})_3$[146] and $LaTiO_2N$.[147] In this study they demonstrated, *via* density functional theory calculations, the potential of suppressing the recombination phenomena of the charge carriers due to the out-of-plane spontaneous polarization that has risen from the epitaxial strain on the anion order within the structure. Experimental studies on $Sr_6Cd_2Sb_6O_7S_{10}$[142] and $Sr_2Sb_2O_2Q_3$ (Q = S, Se)[149] provide a direct comparison of polar *vs.* non-polar structures and different coordination environments for the same cation, supporting this theoretical proposal. $Sr_6Cd_2Sb_6O_7S_{10}$, with its polar structure and zigzag $[CdSb_2OS_5]$ layers, exhibits built-in polarization fields that enhance charge separation and suppress recombination, as confirmed by its strong photocurrent response. In contrast, $Sr_2Sb_2O_2Q_3$, despite its layered but non-centrosymmetric structure, lacks significant internal polarization and relies solely on heteroleptic $SbOQ_4$ coordination, leading to high charge mobility but weaker polarization-driven separation. Thus, the presence of polar distortions, can indeed be a promising route to adopt for increasing the band gap and design new materials with efficient photocatalytic properties.

In this review, we have focused on structural and electronic features which may determine the water-splitting photocatalytic properties of active oxychalcogenides. However, for some of the oxysulfides discussed there are several further studies with drastic enhancement of the H_2 production based on different strategies to those mentioned above including optimization of surface morphology (some of which is covered in specific

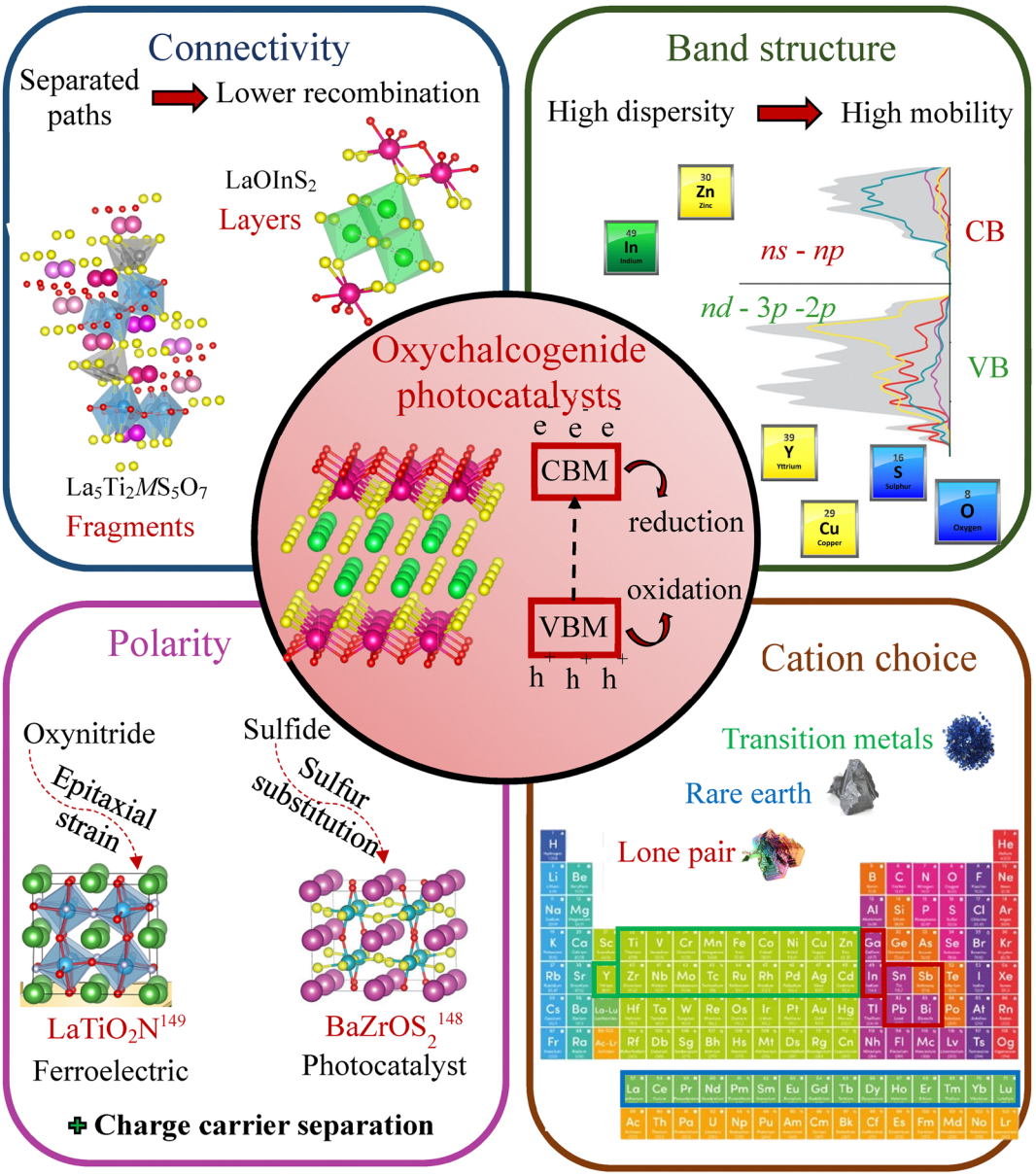

Fig. 12 Schematic diagram of a potential design strategy for oxysulfide photocatalysts.

reviews dealing with the photocatalytic measurement design and optimization of the photocatalysts/co-catalysts). The example of $Gd_2Ti_2S_2O_5$ or $Y_2Ti_2S_2O_5$ for instance, where the particle size and shape and the surface engineering allow drastic enhancement of H_2 release, are very informative.[85,88] The role of defects can also vary by being either counter-productive or helpful such as defect-$(Bi,Ce)_2(O,S)_{3-x}$ nanorods[118] where the multi-valence states and the surface defects facilitate the kinetic reactions, here the defects are controlled and induced during the synthetic process by reduction using hydrazine to incorporate oxygen vacancies. Therefore, beyond intrinsic properties, there is the synthesis design, the cocatalysts type and their interaction with the photocatalyst which play also a crucial role and should be fully considered when designing a photocatalyst. Depending on how the later aspects are handled, the activity might be hampered or improved.

While our review is centered on photocatalytic water splitting, a highly demanding reaction that requires precise band alignment, efficient charge separation, and strong stability under illumination and in aqueous conditions, other types of photocatalytic applications such as CO_2 photoreduction demonstrate the versatility of these materials.[150] However, these alternative photocatalytic processes remain relatively underexplored for oxychalcogenides and we hope our additions will also encourage further investigation beyond water splitting.

It is also interesting to consider the potential of hybrid compounds explicitly combining (oxy)chalcogenides with organic components which are extremely limited. There are a

few instructive examples involving chalcogen elements in hybrid systems. For instance, metal–organic chalcogenide semiconductor nanocrystals have demonstrated the feasibility of incorporating soft chalcogen ligands into hybrid materials.[151] The later study describes metal-chalcogenide layers stacked with organic ligand layers; both layers can be altered to tune the properties. Another example includes a cystamine-based hybrid perovskite, where noncovalent chalcogen bonding involving the cystamine disulfide bridges influences the structure and properties.[152] These studies show that combining soft chalcogen chemistry with organic–inorganic frameworks is chemically viable and could inspire future exploration in oxychalcogenide-based hybrids that may be useful in the photocatalytic field.

A broader overview of these approaches is presented in a review about the current status and future of organic–inorganic hybrid perovskites for photoelectrocatalysis devices,[153] which discusses both hybrid molecular systems and composite architectures used in water-splitting. It highlights how the integration of organic macromolecules (such as oligomers, polymers, or MOFs) with inorganic frameworks can provide synergistic benefits, including improved photocatalytic activity, enhanced stability, and interfacial tunability. On another hand, it is interesting to consider the design of hybrid (composite) photocatalysts that integrate oxychalcogenides with additional materials to form heterostructures or tandem systems. These systems can enhance light absorption, extend charge carrier lifetimes, or spatially separate redox reactions. For example, recent studies report hybrid nanostructures of PBA (Prussian blue analogues) nanocubes wrapped with transition-metal oxysulfides and all together grafted on CC (carbon cloth) substrate (PBA@Co–W–O–S/CC heterostructure), as efficient OER electrocatalysts.[154] Besides, the dye modified Bi_2O_2S/In_2O_3 showed promise for the catalysis of water splitting thanks to the formation of a heterojunction between the oxide-chalcogenide and In_2O_3.[155] Although such strategies are promising, our review deliberately focuses on single-phase oxychalcogenide materials, aiming to clarify intrinsic structure–composition–property relationships without convolution from multicomponent effects. Nonetheless, we now briefly acknowledge these composite designs as a complementary future strategy for improving photocatalytic performance. Lastly, it is interesting to mention theoretical prediction of fully inorganic, single-phase oxychalcogenides as a good alternative to hybrids and oxides in photovoltaics with an enhanced shift current. The authors put forward this strategy to reinforce the idea that simplifying material systems, rather than increasing complexity, can also be a viable and appealing route when structural and electronic requirements are met.[156]

4. Conclusion

In this review, we discussed the concept of photocatalytic water splitting alongside the necessary requirements for a successful reaction in the solar light with a specific focus on layered oxychalcogenides (oxysulfides and oxyselenides). We discussed several oxysulfide materials that are known for their capacity to split water, comparing their different structures and connectivities, band gaps (direct or indirect), semiconduction types (n or p-type), polarity as well as their photocatalytic activity (O_2 and/or H_2 evolution, solar or UV irradiation). This allowed us to extract some key features that can be beneficial for designing new photocatalysts and to propose a potential design strategy for photocatalytic oxychalcogenides consisting on several key points which are exploring the polarity, anion ratio, cation choice (transition metals, lone pairs cations) and connectivity regarding what was reported in the literature; and further work is needed for polarity as well as morphology.

Conflicts of interest

There are no conflicts to declare.

Data availability

No primary research results, software or code have been included and no new data were generated or analysed as part of this review.

Acknowledgements

I-Site (ULNE), University of Lille and University of Kent are thanked for cotutelle funding (S. Al Bacha). Durham University is thanked for hosting research visit. Dr Donna Arnold is thanked for helpful discussions. This study was supported by the French government through the Programme Investissement d'Avenir (I-SITE ULNE/ANR-16-IDEX-0004 ULNE) managed by the Agence Nationale de la Recherche (Project ANION-COMBO).

References

1 A. Nzihou, G. Flamant and B. Stanmore, Synthetic Fuels from Biomass Using Concentrated Solar Energy–a Review, *Energy*, 2012, **42**(1), 121–131.
2 Y. Yang, R. Zhao, T. Zhang, K. Zhao, P. Xiao, Y. Ma, P. M. Ajayan, G. Shi and Y. Chen, Graphene-Based Standalone Solar Energy Converter for Water Desalination and Purification, *ACS Nano*, 2018, **12**(1), 829–835.
3 S. Mekhilef, R. Saidur and A. Safari, A Review on Solar Energy Use in Industries, *Renewable Sustainable Energy Rev.*, 2011, **15**(4), 1777–1790.
4 B. Martinez, A. Roig, X. Obradors, E. Molins, A. Rouanet and C. Monty, Magnetic Properties of γ-Fe2O3 Nanoparticles Obtained by Vaporization Condensation in a Solar Furnace, *J. Appl. Phys.*, 1996, **79**(5), 2580–2586.
5 J. Qi, W. Zhang and R. Cao, Solar-to-hydrogen Energy Conversion Based on Water Splitting, *Adv. Energy Mater.*, 2018, **8**(5), 1701620.
6 P. Zhang and X. W. Lou, Design of Heterostructured Hollow Photocatalysts for Solar-to-chemical Energy Conversion, *Adv. Mater.*, 2019, **31**(29), 1900281.
7 T. Shiyani, S. Agrawal and I. Banerjee, Natural-Dye-Sensitized Photoelectrochemical Cells for Solar Energy Conversion, *Nanomater. Energy*, 2020, **9**(2), 215–226.
8 C. F. Goodeve and J. A. Kitchener, Photosensitisation by Titanium Dioxide, *Trans. Faraday Soc.*, 1938, **34**, 570–579.

9 K. Hashimoto, H. Irie and A. Fujishima, TiO_2 Photocatalysis: A Historical Overview and Future Prospects, *Jpn. J. Appl. Phys.*, 2005, **44**(12R), 8269.
10 A. Fujishima and K. Honda, Electrochemical Photolysis of Water at a Semiconductor Electrode, *Nature*, 1972, **238**(5358), 37–38.
11 A. Fujishima, T. N. Rao and D. A. Tryk, Titanium Dioxide Photocatalysis, *J. Photochem. Photobiol., C*, 2000, **1**(1), 1–21.
12 A. Fujishima, X. Zhang and D. A. Tryk, TiO2 Photocatalysis and Related Surface Phenomena, *Surf. Sci. Rep.*, 2008, **63**(12), 515–582.
13 K. Hashimoto, H. Irie and A. Fujishima, TiO_2 Photocatalysis: A Historical Overview and Future Prospects, *Jpn. J. Appl. Phys.*, 2005, **44**(12R), 8269.
14 S. Leroy, Etude Des Propriétés Photocatalytiques et Photoélectriques Du Dititanate de Lanthane (La2Ti2O7) à Structure Pérovskite En Feuillets et Son Utilisation Dans Des Hétérojonctions Tout Oxyde Pour La Conversion d'énergie, Thèse de doctorat, Université d'Artois, 2020.
15 T. Jafari, E. Moharreri, A. S. Amin, R. Miao, W. Song and S. L. Suib, Photocatalytic Water Splitting—the Untamed Dream: A Review of Recent Advances, *Molecules*, 2016, **21**(7), 900.
16 Z. Liang, C.-F. Yan, S. Rtimi and J. Bandara, Piezoelectric Materials for Catalytic/Photocatalytic Removal of Pollutants: Recent Advances and Outlook, *Appl. Catal., B*, 2019, **241**, 256–269.
17 M. Wang, B. Wang, F. Huang and Z. Lin, Enabling PIEZOpotential in PIEZOelectric Semiconductors for Enhanced Catalytic Activities, *Angew. Chem., Int. Ed.*, 2019, **58**(23), 7526–7536, DOI: **10.1002/anie.201811709**.
18 F. Chen, H. Huang, L. Guo, Y. Zhang and T. Ma, The Role of Polarization in Photocatalysis, *Angew. Chem., Int. Ed.*, 2019, **58**(30), 10061–10073.
19 E. D. Wachsman and K. T. Lee, Lowering the Temperature of Solid Oxide Fuel Cells, *Science*, 2011, **334**(6058), 935–939, DOI: **10.1126/science.1204090**.
20 A. Staykov; S. M. Lyth and M. Watanabe, Photocatalytic Water Splitting, *Hydrogen Energy Engineering*, Springer, 2016, pp. 159–174.
21 D. Kong, Y. Zheng, M. Kobielusz, Y. Wang, Z. Bai, W. Macyk, X. Wang and J. Tang, Recent Advances in Visible Light-Driven Water Oxidation and Reduction in Suspension Systems, *Mater. Today*, 2018, **21**(8), 897–924.
22 Y. Luan, Y. Li, Z. Li, B. Y. Zhang and J. Z. Ou, Layered Anion-Mixed Oxycompounds: Synthesis, Properties, and Applications, *Adv. Sci.*, 2025, **12**, 2500477, DOI: **10.1002/advs.202500477**.
23 M. Li, N. Wang, S. Zhang, J. Hu, H. Xiao, H. Gong, Z. Liu, L. Qiao and X. Zu, A Review of the Properties, Synthesis and Applications of Lanthanum Copper Oxychalcogenides, *J. Phys. D:Appl. Phys.*, 2022, **55**(27), 273002, DOI: **10.1088/1361-6463/ac4b71**.
24 S. J. Clarke, P. Adamson, S. J. Herkelrath, O. J. Rutt, D. R. Parker, M. J. Pitcher and C. F. Smura, Structures, Physical Properties, and Chemistry of Layered Oxychalcogenides and Oxypnictides, *Inorg. Chem.*, 2008, **47**(19), 8473–8486.
25 Y. Kobayashi, O. Hernandez, C. Tassel and H. Kageyama, New Chemistry of Transition Metal Oxyhydrides, *Sci. Technol. Adv. Mater.*, 2017, **18**(1), 905–918.
26 L. Wang, L. Wang, Y. Du, X. Xu and S. X. Dou, Progress and Perspectives of Bismuth Oxyhalides in Catalytic Applications, *Mater. Today Phys.*, 2021, **16**, 100294.
27 A. Nakada, D. Kato, R. Nelson, H. Takahira, M. Yabuuchi, M. Higashi, H. Suzuki, M. Kirsanova, N. Kakudou and C. Tassel, Conduction Band Control of Oxyhalides with a Triple-Fluorite Layer for Visible Light Photocatalysis, *J. Am. Chem. Soc.*, 2021, **143**(6), 2491–2499.
28 Y. Li, H. Jiang, X. Wang, X. Hong and B. Liang, Recent Advances in Bismuth Oxyhalide Photocatalysts for Degradation of Organic Pollutants in Wastewater, *RSC Adv.*, 2021, **11**(43), 26855–26875.
29 E. J. Cho, S.-J. Oh, H. Jo, J. Lee, T.-S. You and K. M. Ok, Layered Bismuth Oxyfluoride Nitrates Revealing Large Second-Harmonic Generation and Photocatalytic Properties, *Inorg. Chem.*, 2019, **58**(3), 2183–2190.
30 Y. Kobayashi, Y. Tang, T. Kageyama, H. Yamashita, N. Masuda, S. Hosokawa and H. Kageyama, Titanium-Based Hydrides as Heterogeneous Catalysts for Ammonia Synthesis, *J. Am. Chem. Soc.*, 2017, **139**(50), 18240–18246.
31 M. Ai-Mamouri, P. P. Edwards, C. Greaves and M. Slaski, Synthesis and Superconducting Properties of the Strontium Copper Oxy-Fluoride Sr2CuO2F2+δ, *Nature*, 1994, **369**(6479), 382–384.
32 Y. Kamihara, H. Hiramatsu, M. Hirano, R. Kawamura, H. Yanagi, T. Kamiya and H. Hosono, Iron-Based Layered Superconductor: LaOFeP, *J. Am. Chem. Soc.*, 2006, **128**(31), 10012–10013.
33 Y. Kamihara, T. Watanabe, M. Hirano and H. Hosono, Iron-Based Layered Superconductor La [O1-x F x] FeAs (X = 0.05− 0.12) with T C = 26 K, *J. Am. Chem. Soc.*, 2008, **130**(11), 3296–3297.
34 R. K. Oogarah, E. Suard and E. E. McCabe, Magnetic Order and Phase Transition in the Iron Oxysulfide La2O2Fe2OS2, *J. Magn. Magn. Mater.*, 2018, **446**, 101–107.
35 S. Okada, M. Matoba, S. Fukumoto, S. Soyano, Y. Kamihara, T. Takeuchi, H. Yoshida, K. Ohoyama and Y. Yamaguchi, Magnetic Properties of Layered Oxysulfide Sr 2 Cu 2 (Co, Cu) O 2 S 2 with Cu-Doped CoO 2 Square Planes, *J. Appl. Phys.*, 2002, **91**(10), 8861–8863.
36 F. M. Ryan, E. W. Pugh and R. Smoluchowski, Superparamagnetism, Nonrandomness, and Irradiation Effects in Cu-Ni Alloys, *Phys. Rev.*, 1959, **116**(5), 1106.
37 Y.-Y. Li, W.-J. Wang, H. Wang, H. Lin and L.-M. Wu, Mixed-Anion Inorganic Compounds: A Favorable Candidate for Infrared Nonlinear Optical Materials, *Cryst. Growth Des.*, 2019, **19**(7), 4172–4192.
38 F. Sauvage, V. Bodenez, H. Vezin, T. A. Albrecht, J.-M. Tarascon and K. R. Poeppelmeier, Ag4V2O6F2 (SVOF): A High Silver Density Phase and Potential New Cathode Material for Implantable Cardioverter Defibrillators, *Inorg. Chem.*, 2008, **47**(19), 8464–8472.
39 J. Li, W. Zhai, C. Zhang, Y. Yan, P.-F. Liu and G. Yang, Anharmonicity and Ultralow Thermal Conductivity in Layered Oxychalcogenides BiAgOCh (Ch= S, Se, and Te), *Mater. Adv.*, 2021, **2**(14), 4876–4882.
40 N. Hirosaki, R.-J. Xie, K. Kimoto, T. Sekiguchi, Y. Yamamoto, T. Suehiro and M. Mitomo, Characterization and Properties of Green-Emitting β-SiAlON: Eu 2+ Powder Phosphors for White Light-Emitting Diodes, *Appl. Phys. Lett.*, 2005, **86**(21), 211905.
41 H. Kageyama, K. Hayashi, K. Maeda, J. P. Attfield, Z. Hiroi, J. M. Rondinelli and K. R. Poeppelmeier, Expanding Frontiers in Materials Chemistry and Physics with Multiple Anions, *Nat. Commun.*, 2018, **9**(1), 1–15.
42 J. P. Attfield, Principles and Applications of Anion Order in Solid Oxynitrides, *Cryst. Growth Des.*, 2013, **13**(10), 4623–4629.
43 G. Shi, Y., S. Yu, A. Belik, A., Y. Matsushita, M. Tanaka, Y. Katsuya, K. Kobayashi, K. Yamaura and E. Takayama-Muromachi, Synthesis and Superconducting Properties of the Iron Oxyarsenide TbFeAsO0.85, *J. Phys. Soc. Jpn.*, 2008, **77**(Suppl. C), 155–157.
44 S. V. Chong, T. Mochiji and K. Kadowaki, Superconductivity in Yttrium Iron Oxyarsenide System, *Journal of Physics: Conference Series*, IOP Publishing, 2009, vol. 150, p. 052036.
45 M. Orr, G. R. Hebberd, E. E. McCabe and R. T. Macaluso, Structural Diversity of Rare-Earth Oxychalcogenides, *ACS Omega*, 2022, **7**(10), 8209–8218.
46 S. D. Luu and P. Vaqueiro, Layered Oxychalcogenides: Structural Chemistry and Thermoelectric Properties, *J. Materiomics*, 2016, **2**(2), 131–140.
47 Y.-F. Shi, W.-B. Wei, X.-T. Wu, H. Lin and Q.-L. Zhu, Recent Progress in Oxychalcogenides as IR Nonlinear Optical Materials, *Dalton Trans.*, 2021, **50**(12), 4112–4118.
48 A. Parida, S. Senapati and R. Naik, Recent Developments on Bi-Based Oxychalcogenide Materials with Thermoelectric and Optoelectronic Applications: An Overview, *Mater. Today Chem.*, 2022, **26**, 101149.
49 K. Maeda and K. Domen, New Non-Oxide Photocatalysts Designed for Overall Water Splitting under Visible Light, *J. Phys. Chem. C*, 2007, **111**(22), 7851–7861, DOI: **10.1021/jp070911w**.
50 T. Takata and K. Domen, Development of Non-Oxide Semiconductors as Light Harvesting Materials in Photocatalytic and Photoelectrochemical Water Splitting, *Dalton Trans.*, 2017, **46**(32), 10529–10544.
51 A. Miyoshi and K. Maeda, Recent Progress in Mixed-Anion Materials for Solar Fuel Production, *Sol. RRL*, 2021, **5**(6), 2000521.
52 K. Chatterjee and S. E. Skrabalak, Durable Metal Heteroanionic Photocatalysts, *ACS Appl. Mater. Interfaces*, 2021, **13**(31), 36670–36678, DOI: **10.1021/acsami.1c09774**.
53 Y. Subramanian, A. Dhanasekaran, L. A. Omeiza, M. R. Somalu and A. K. Azad, A Review on Heteroanionic-Based Materials for Photocatalysis Applications, *Catalysts*, 2023, **13**(1), 173.
54 E. J. Salter, J. N. Blandy and S. J. Clarke, Crystal and Magnetic Structures of the Oxide Sulfides CaCoSO and BaCoSO, *Inorg. Chem.*, 2016, **55**(4), 1697–1701.

55 K. Shah, A. Ćirić, K. V. R. Murthy and B. S. Chakrabarty, Investigation of a New Way of Synthesis for Nano Crystallites of La2O2S & 1% Ln3+ (Ln = Pr, Eu, Tb, Dy, Er) Doped La2O2S and Study Their Structural and Optical Properties, *J. Alloys Compd.*, 2021, **851**, 156725.
56 S. Strobel, A. Choudhury, P. K. Dorhout, C. Lipp and T. Schleid, Rare-Earth Metal (III) Oxide Selenides M4O4Se [Se2](M = La, Ce, Pr, Nd, Sm) with Discrete Diselenide Units: Crystal Structures, Magnetic Frustration, and Other Properties, *Inorg. Chem.*, 2008, **47**(11), 4936–4944.
57 V. Johnson and W. Jeitschko, ZrCuSiAs: A ''Filled'' PbFCl Type, *J. Solid State Chem.*, 1974, **11**(2), 161–166.
58 W. A. Phelan, D. C. Wallace, K. E. Arpino, J. R. Neilson, K. J. Livi, C. R. Seabourne, A. J. Scott and T. M. McQueen, Stacking Variants and Superconductivity in the Bi–O–S System, *J. Am. Chem. Soc.*, 2013, **135**(14), 5372–5374.
59 K. Ueda, H. Hiramatsu, M. Hirano, T. Kamiya and H. Hosono, Wide-Gap Layered Oxychalcogenide Semiconductors: Materials, Electronic Structures and Optoelectronic Properties, *Thin Solid Films*, 2006, **496**(1), 8–15.
60 M. Palazzi, C. Carcaly, P. Laruelle and J. Flahaut, Crystal Structure and Properties of (LaO) CuS and (LaO) AgS, *The Rare Earths in Modern Science and Technology*, Springer, 1982, pp. 347–350.
61 L.-D. Zhao, J. He, D. Berardan, Y. Lin, J.-F. Li, C.-W. Nan and N. Dragoe, BiCuSeO Oxyselenides: New Promising Thermoelectric Materials, *Energy Environ. Sci.*, 2014, **7**(9), 2900–2924.
62 J.-X. Zhu, R. Yu, H. Wang, L. L. Zhao, M. D. Jones, J. Dai, E. Abrahams, E. Morosan, M. Fang and Q. Si, Band Narrowing and Mott Localization in Iron Oxychalcogenides $La_2O_2Fe_2OSeS_2$, *Phys. Rev. Lett.*, 2010, **104**(21), 216405, DOI: **10.1103/PhysRevLett.104.216405**.
63 M. Lü, O. Mentré, E. E. Gordon, M.-H. Whangbo, A. Wattiaux, M. Duttine, N. Tiercelin and H. Kabbour, A Comprehensive Study of Magnetic Exchanges in the Layered Oxychalcogenides Sr3Fe2O5-Cu2Q2 (Q = S, Se), *J. Magn. Magn. Mater.*, 2017, **444**, 147–153, DOI: **10.1016/j.jmmm.2017.07.026**.
64 E. E. McCabe, D. G. Free, B. G. Mendis, J. S. Higgins and J. S. Evans, Preparation, Characterization, and Structural Phase Transitions in a New Family of Semiconducting Transition Metal Oxychalcogenides β-La2O2 M Se2 (M = Mn, Fe), *Chem. Mater.*, 2010, **22**(22), 6171–6182.
65 Z. A. Gál, O. J. Rutt, C. F. Smura, T. P. Overton, N. Barrier, S. J. Clarke and J. Hadermann, Structural Chemistry and Metamagnetism of an Homologous Series of Layered Manganese Oxysulfides, *J. Am. Chem. Soc.*, 2006, **128**(26), 8530–8540.
66 A. H. Reshak, CaCoSO Diluted Magnetic Antiferromagnet Semiconductor as Efficient Thermoelectric Materials, *Mater. Res. Bull.*, 2017, **94**, 22–30.
67 Y.-F. Shi, W.-B. Wei, X.-T. Wu, H. Lin and Q.-L. Zhu, Recent Progress in Oxychalcogenides as IR Nonlinear Optical Materials, *Dalton Trans.*, 2021, **50**(12), 4112–4118.
68 B.-W. Liu, X.-M. Jiang, G.-E. Wang, H.-Y. Zeng, M.-J. Zhang, S.-F. Li, W.-H. Guo and G.-C. Guo, Oxychalcogenide BaGeOSe2: Highly Distorted Mixed-Anion Building Units Leading to a Large Second-Harmonic Generation Response, *Chem. Mater.*, 2015, **27**(24), 8189–8192.
69 W. Xing, P. Fang, N. Wang, Z. Li, Z. Lin, J. Yao, W. Yin and B. Kang, Two Mixed-Anion Units of [GeOSe3] and [GeO3S] Originating from Partial Isovalent Anion Substitution and Inducing Moderate Second Harmonic Generation Response and Large Birefringence, *Inorg. Chem.*, 2020, **59**(22), 16716–16724.
70 B.-W. Liu, X.-M. Jiang, G.-E. Wang, H.-Y. Zeng, M.-J. Zhang, S.-F. Li, W.-H. Guo and G.-C. Guo, Oxychalcogenide BaGeOSe2: Highly Distorted Mixed-Anion Building Units Leading to a Large Second-Harmonic Generation Response, *Chem. Mater.*, 2015, **27**(24), 8189–8192.
71 R. Wang, F. Liang, F. Wang, Y. Guo, X. Zhang, Y. Xiao, K. Bu, Z. Lin, J. Yao and T. Zhai, Sr6Cd2Sb6O7S10: Strong SHG Response Activated by Highly Polarizable Sb/O/S Groups, *Angew. Chem., Int. Ed.*, 2019, **58**(24), 8078–8081.
72 Y. Wang, M. Luo, P. Zhao, X. Che, Y. Cao and F. Huang, Sr 4 Pb 1.5 Sb 5 O 5 Se 8: A New Mid-Infrared Nonlinear Optical Material with a Moderate SHG Response, *CrystEngComm*, 2020, **22**(20), 3526–3530.
73 R. Wang, F. Wang, X. Zhang, X. Feng, C. Zhao, K. Bu, Z. Zhang, T. Zhai and F. Huang, Improved Polarization in the Sr6Cd2Sb6-O7Se10 Oxyselenide through Design of Lateral Sublattices for Efficient Photoelectric Conversion, *Angew. Chem.*, 2022, **61**(33), e202206816, DOI: **10.1002/anie.202206816**.
74 W. J. Zhu and P. H. Hor, Unusual Layered Transition-Metal Oxysulfides: Sr2Cu2MO2S2 (M = Mn, Zn), *J. Solid State Chem.*, 1997, **130**(2), 319–321.
75 W. J. Zhu and P. H. Hor, Sr2CuGaO3S, a Rare Example of Square Pyramidal Gallium, *Inorg. Chem.*, 1997, **36**(17), 3576–3577.
76 M. Guittard, S. Benazeth, J. Dugue, S. Jaulmes, M. Palazzi, P. Laruelle and J. Flahaut, Oxysulfides and Oxyselenides in Sheets, Formed by a Rare Earth Element and a Second Metal, *J. Solid State Chem.*, 1984, **51**(2), 227–238.
77 T. Sambrook, C. F. Smura, S. J. Clarke, K. M. Ok and P. S. Halasyamani, Structure and Physical Properties of the Polar Oxysulfide CaZnOS, *Inorg. Chem.*, 2007, **46**(7), 2571–2574.
78 C. Boyer, C. Deudon and A. Meerschaut, Synthesis and Structure Determination of the New Sm2Ti2O5S2 Compound, *C. R. Acad. Sci., Ser. IIc: Chim.*, 1999, **2**(2), 93–99, DOI: **10.1016/S1387-1609(99)80007-3**.
79 M. Goga, R. Seshadri, V. Ksenofontov, P. Gütlich and W. Tremel, Ln 2 Ti 2 S 2 O 5 (Ln = Nd, Pr, Sm): A Novel Series of Defective Ruddlesden–Popper Phases, *Chem. Commun.*, 1999, 979–980.
80 C. Boyer-Candalen, J. Derouet, P. Porcher, Y. Moëlo and A. Meerschaut, The Family of Ln2Ti2S2O5 Compounds (Ln = Nd, Sm, Gd, Tb, Dy, Ho, Er, and Y): Optical Properties, *J. Solid State Chem.*, 2002, **165**(2), 228–237.
81 A. Ishikawa, T. Takata, T. Matsumura, J. N. Kondo, M. Hara, H. Kobayashi and K. Domen, Oxysulfides Ln2Ti2S2O5 as Stable Photocatalysts for Water Oxidation and Reduction under Visible-Light Irradiation, *J. Phys. Chem. B*, 2004, **108**(8), 2637–2642.
82 A. Ishikawa, T. Takata, J. N. Kondo, M. Hara, H. Kobayashi and K. Domen, Oxysulfide Sm2Ti2S2O5 as a Stable Photocatalyst for Water Oxidation and Reduction under Visible Light Irradiation ($\Lambda \leq 650$ Nm), *J. Am. Chem. Soc.*, 2002, **124**(45), 13547–13553.
83 A. Ishikawa, Y. Yamada, T. Takata, J. N. Kondo, M. Hara, H. Kobayashi and K. Domen, Novel Synthesis and Photocatalytic Activity of Oxysulfide Sm2Ti2S2O5, *Chem. Mater.*, 2003, **15**(23), 4442–4446.
84 J. Zhang, K. Liu, B. Zhang, J. Zhang, M. Liu, Y. Xu, K. Shi, H. Wang, Z. Zhang, P. Zhou and G. Ma, Anisotropic Charge Migration on Perovskite Oxysulfide for Boosting Photocatalytic Overall Water Splitting, *J. Am. Chem. Soc.*, 2024, **146**(6), 4068–4077, DOI: **10.1021/jacs.3c12417**.
85 Q. Wang, M. Nakabayashi, T. Hisatomi, S. Sun, S. Akiyama, Z. Wang, Z. Pan, X. Xiao, T. Watanabe and T. Yamada, Oxysulfide Photocatalyst for Visible-Light-Driven Overall Water Splitting, *Nat. Mater.*, 2019, **18**(8), 827–832.
86 H. Yoshida, Z. Pan, R. Shoji, V. Nandal, H. Matsuzaki, K. Seki, T. Hisatomi and K. Domen, Heterogeneous Doping of Visible-Light-Responsive Y2Ti2O5S2 for Enhanced Hydrogen Evolution, *J. Mater. Chem. A*, 2022, **10**(46), 24552–24560, DOI: **10.1039/D2TA06895H**.
87 L. Lin, M. Nakabayashi, D. Lu, T. Hisatomi, T. Takata and K. Domen, Formation Mechanism for Particulate Y2Ti2O5S2 Photocatalyst by the Solid-State Reaction, *Chem. Mater.*, 2024, **36**(3), 1612–1620, DOI: **10.1021/acs.chemmater.3c02929**.
88 H. Yoshida, Z. Pan, R. Shoji, V. Nandal, H. Matsuzaki, K. Seki, L. Lin, M. Kaneko, T. Fukui, K. Yamashita, T. Takata, T. Hisatomi and K. Domen, An Oxysulfide Photocatalyst Evolving Hydrogen with an Apparent Quantum Efficiency of 30% under Visible Light, *Angew. Chem.*, 2023, **135**(46), e202312938, DOI: **10.1002/ange.202312938**.
89 H. Yoshida, Z. Pan, R. Shoji, V. Nandal, H. Matsuzaki, K. Seki, L. Lin, M. Kaneko, T. Fukui, K. Yamashita, T. Takata, T. Hisatomi and K. Domen, An Oxysulfide Photocatalyst Evolving Hydrogen with an Apparent Quantum Efficiency of 30% under Visible Light, *Angew. Chem.*, 2023, **135**(46), e202312938, DOI: **10.1002/ange.202312938**.
90 Y. Tsujimoto, C. A. Juillerat, W. Zhang, K. Fujii, M. Yashima, P. S. Halasyamani and H.-C. zur Loye, Function of Tetrahedral ZnS3O Building Blocks in the Formation of SrZn2S2O: A Phase Matchable Polar Oxysulfide with a Large Second Harmonic Generation Response, *Chem. Mater.*, 2018, **30**(18), 6486–6493.

91 A. H. Reshak, Sulfide Oxide XZnSO (X = Ca or Sr) as Novel Active Photocatalytic Water Splitting Solar-to-Hydrogen Energy Conversion, *Appl. Catal., B*, 2018, **225**, 273–283.
92 S. Nishioka, T. Kanazawa, K. Shibata, Y. Tsujimoto, H.-C. Zur Loye and K. Maeda, A Zinc-Based Oxysulfide Photocatalyst SrZn 2 S 2 O Capable of Reducing and Oxidizing Water, *Dalton Trans.*, 2019, **48**(42), 15778–15781.
93 H. Kabbour, L. Cario, Y. Moëlo and A. Meerschaut, Synthesis, X-Ray and Optical Characterizations of Two New Oxysulfides: LaInS2O and La5In3S9O3, *J. Solid State Chem.*, 2004, **177**(4–5), 1053–1059.
94 H. Kabbour, A. Sayede, S. Saitzek, G. Lefevre, L. Cario, M. Trentesaux and P. Roussel, Structure of the Water-Splitting Photocatalyst Oxysulfide α-LaOInS 2 and Ab Initio Prediction of New Polymorphs, *Chem. Commun.*, 2020, **56**(11), 1645–1648.
95 A. Miura, T. Oshima, K. Maeda, Y. Mizuguchi, C. Moriyoshi, Y. Kuroiwa, Y. Meng, X.-D. Wen, M. Nagao and M. Higuchi, Synthesis, Structure and Photocatalytic Activity of Layered LaOInS 2, *J. Mater. Chem. A*, 2017, **5**(27), 14270–14277.
96 H. Ito, A. Miura, Y. Goto, Y. Mizuguchi, C. Moriyoshi, Y. Kuroiwa, M. Azuma, J. Liu, X.-D. Wen and S. Nishioka, An Electronic Structure Governed by the Displacement of the Indium Site in In–S 6 Octahedra: LnOInS 2 (Ln = La, Ce, and Pr), *Dalton Trans.*, 2019, **48**(32), 12272–12278.
97 M. Machida, S. Murakami, T. Kijima, S. Matsushima and M. Arai, Photocatalytic Property and Electronic Structure of Lanthanide Tantalates, LnTaO4 (Ln = La, Ce, Pr, Nd, and Sm), *J. Phys. Chem. B*, 2001, **105**(16), 3289–3294.
98 H. Wakayama, K. Hibino, K. Fujii, T. Oshima, K. Yanagisawa, Y. Kobayashi, K. Kimoto, M. Yashima and K. Maeda, Synthesis of a Layered Niobium Oxynitride, Rb2NdNb2O6N· H2O, Showing Visible-Light Photocatalytic Activity for H2 Evolution, *Inorg. Chem.*, 2019, **58**(9), 6161–6166.
99 L. Gastaldi, D. Carre and M. P. Pardo, Structure de l'oxysulfure d'indium et de Lanthane In6La10O6S17, *Acta Crystallogr., Sect. B*, 1982, **38**(9), 2365–2367.
100 K. Ogisu, A. Ishikawa, K. Teramura, K. Toda, M. Hara and K. Domen, Lanthanum–Indium Oxysulfide as a Visible Light Driven Photocatalyst for Water Splitting, *Chem. Lett.*, 2007, **36**(7), 854–855.
101 S. Jaulmes, Oxysulfure de Gallium et de Lanthane LaGaOS2, *Acta Crystallogr., Sect. B*, 1978, **34**(8), 2610–2612.
102 S. Jaulmes, A. Mazurier and M. Guittard, Structure de l'oxypentasulfure de Gallium et de Trilanthane, GaLa3OS5, *Acta Crystallogr., Sect. C: Cryst. Struct. Commun.*, 1983, **39**(12), 1594–1597.
103 K. Ogisu, A. Ishikawa, Y. Shimodaira, T. Takata, H. Kobayashi and K. Domen, Electronic Band Structures and Photochemical Properties of La–Ga-Based Oxysulfides, *J. Phys. Chem. C*, 2008, **112**(31), 11978–11984.
104 V. Meignen, L. Cario, A. Lafond, Y. Moëlo, C. Guillot-Deudon and A. Meerschaut, Crystal Structures of Two New Oxysulfides La5Ti2MS5O7 (M = Cu, Ag): Evidence of Anionic Segregation, *J. Solid State Chem.*, 2004, **177**(8), 2810–2817.
105 M. Katayama, D. Yokoyama, Y. Maeda, Y. Ozaki, M. Tabata, Y. Matsumoto, A. Ishikawa, J. Kubota and K. Domen, Fabrication and Photoelectrochemical Properties of La5Ti2MS5O7 (M= Ag, Cu) Electrodes, *Mater. Sci. Eng., B*, 2010, **173**(1–3), 275–278.
106 T. Suzuki, T. Hisatomi, K. Teramura, Y. Shimodaira, H. Kobayashi and K. Domen, A Titanium-Based Oxysulfide Photocatalyst: La 5 Ti 2 MS 5 O 7 (M= Ag, Cu) for Water Reduction and Oxidation, *Phys. Chem. Chem. Phys.*, 2012, **14**(44), 15475–15481.
107 J. Liu, T. Hisatomi, G. Ma, A. Iwanaga, T. Minegishi, Y. Moriya, M. Katayama, J. Kubota and K. Domen, Improving the Photoelectrochemical Activity of La5Ti2CuS5O7 for Hydrogen Evolution by Particle Transfer and Doping, *Energy Environ. Sci.*, 2014, **7**(7), 2239–2242.
108 G. Ma, Y. Suzuki, R. B. Singh, A. Iwanaga, Y. Moriya, T. Minegishi, J. Liu, T. Hisatomi, H. Nishiyama and M. Katayama, Photoanodic and Photocathodic Behaviour of La 5 Ti 2 CuS 5 O 7 Electrodes in the Water Splitting Reaction, *Chem. Sci.*, 2015, **6**(8), 4513–4518.
109 H. Hirose, K. Ueda, H. Kawazoe and H. Hosono, Electronic Structure of Sr2Cu2ZnO2S2 Layered Oxysulfide with CuS Layers, *Chem. Mater.*, 2002, **14**(3), 1037–1041.
110 S. Nandy, T. Hisatomi, M. Katayama, T. Minegishi and K. Domen, Effects of Calcination Temperature on the Physical Properties and Hydrogen Evolution Activities of La5Ti2Cu(S1-Se)5O7 Photocatalysts, *Part. Part. Syst. Charact.*, 2018, **35**(1), 1700275, DOI: **10.1002/ppsc.201700275**.
111 Z. Pan, Q. Xiao, S. Chen, Z. Wang, L. Lin, M. Nakabayashi, N. Shibata, T. Takata, T. Hisatomi and K. Domen, Synthesis of a Ga-Doped La5Ti2Cu0.9Ag0.1O7S5 Photocatalyst by Thermal Sulfidation for Hydrogen Evolution under Visible Light, *J. Catal.*, 2021, **399**, 230–236, DOI: **10.1016/j.jcat.2021.05.015**.
112 X. Tang, H. Ye and H. Hu, Sulfurization Synthesis and Photocatalytic Activity of Oxysulfide La3NbS2O5, *Trans. Nonferrous Met. Soc. China*, 2013, **23**(9), 2644–2649, DOI: **10.1016/S1003-6326(13)62780-6**.
113 A. BaQais, A. Curutchet, A. Ziani, H. Ait Ahsaine, P. Sautet, K. Takanabe and T. Le Bahers, Bismuth Silver Oxysulfide for Photoconversion Applications: Structural and Optoelectronic Properties, *Chem. Mater.*, 2017, **29**(20), 8679–8689, DOI: **10.1021/acs.chemmater.7b02664**.
114 M. Ogawa, H. Suzuki, O. Tomita, A. Nakada and R. Abe, Sn^{2+}-Based Pyrochlore Oxysulfides with Narrow Band Gaps for Photocatalytic Water Splitting, *J. Photochem. Photobiol., A*, 2023, **444**, 114895, DOI: **10.1016/j.jphotochem.2023.114895**.
115 K. H. Chu, L. Ye, W. Wang, D. Wu, D. K. L. Chan, C. Zeng, H. Y. Yip, J. C. Yu and P. K. Wong, Enhanced Photocatalytic Hydrogen Production from Aqueous Sulfide/Sulfite Solution by ZnO0.6S0.4 with Simultaneous Dye Degradation under Visible-Light Irradiation, *Chemosphere*, 2017, **183**, 219–228, DOI: **10.1016/j.chemosphere.2017.05.112**.
116 N. S. Gultom, H. Abdullah and D.-H. Kuo, Enhanced Photocatalytic Hydrogen Production of Noble-Metal Free Ni-Doped Zn(O,S) in Ethanol Solution, *Int. J. Hydrogen Energy*, 2017, **42**(41), 25891–25902, DOI: **10.1016/j.ijhydene.2017.08.198**.
117 N. S. Gultom, H. Abdullah, J.-C. Xie, H. Shuwanto and D.-H. Kuo, Improved Hydrogen Production Rate of a Nickel-Doped Zinc Indium Oxysulfide Visible-Light Catalyst: Comparative Study of Stoichiometric and Nonstoichiometric Compounds, *ACS Appl. Energy Mater.*, 2022, **5**(2), 1755–1766, DOI: **10.1021/acsaem.1c03200**.
118 X. Chen, Q. Wu, D.-H. Kuo, A. B. Abdeta, H. Zhang, P. Li, T. Huang, O. A. Zelekew and J. Lin, Initiating Highly Efficient (Bi,Ce)2(O,S)3−x Oxysulfide Catalysts with Rich Oxygen Vacancies for Hydrogen Evolution via Adjusting Valence Band Configuration, *J. Mater. Chem. A*, 2023, **11**(8), 4126–4141, DOI: **10.1039/D2TA09780J**.
119 S. Mallick, F. Orlandi, P. Manuel, W. Zhang, P. S. Halasyamani and M. A. Hayward, MnCaTa2O7—A Magnetically Ordered Polar Phase Prepared *via* Cation Exchange, *Chem. Mater.*, 2023, **35**(18), 7839–7846, DOI: **10.1021/acs.chemmater.3c01850**.
120 H. Yoshida, P. Zhenhua, S. Ryota, M. Vikas, M. Hiroyuki, S. Kazuhiko, H. Takashi and D. Kazunari, Heterogeneous doping of visible-light-responsive Y2Ti2O5S2 for enhanced hydrogen evolution, *J. Mater. Chem. A*, 2022, **10**(46), 24552–24560, DOI: **10.1039/D2TA06895H**.
121 T. Hisatomi, S. Okamura, J. Liu, Y. Shinohara, K. Ueda, T. Higashi, M. Katayama, T. Minegishi and K. Domen, $La_5Ti_2Cu_{1-x}Ag_xS_5O_7$ Photocathodes Operating at Positive Potentials during Photoelectrochemical Hydrogen Evolution under Irradiation of up to 710 Nm, *Energy Environ. Sci.*, 2015, **8**(11), 3354–3362.
122 H. Liang, H. Sun, S. Jiang, S. Cui, F. Song, L. Fan and Q. Xu, Two-Dimensional (2D) Oxysulfide Nanosheets with Sulfur-Rich Vacancy as an Visible-Light-Driven Difunctional Photocatalyst for Hydrogen and Oxygen Evolution, *J. Alloys Compd.*, 2024, **1004**, 175898, DOI: **10.1016/j.jallcom.2024.175898**.
123 J. Cui, C. Li and F. Zhang, Development of Mixed-Anion Photocatalysts with Wide Visible-Light Absorption Bands for Solar Water Splitting, *ChemSusChem*, 2019, **12**(9), 1872–1888.
124 Y. Goto, J. Seo, K. Kumamoto, T. Hisatomi, Y. Mizuguchi, Y. Kamihara, M. Katayama, T. Minegishi and K. Domen, Crystal Structure, Electronic Structure, and Photocatalytic Activity of Oxysulfides: La2Ta2ZrS2O8, La2Ta2TiS2O8, and La2Nb2TiS2O8, *Inorg. Chem.*, 2016, **55**(7), 3674–3679.
125 J. P. Allen, J. J. Carey, A. Walsh, D. O. Scanlon and G. W. Watson, Electronic Structures of Antimony Oxides, *J. Phys. Chem. C*, 2013, **117**(28), 14759–14769.

126 R. Vadapoo, S. Krishnan, H. Yilmaz and C. Marin, Self-Standing Nanoribbons of Antimony Selenide and Antimony Sulfide with Well-Defined Size and Band Gap, *Nanotechnology*, 2011, **22**(17), 175705.
127 F. Liang, L. Kang, Z. Lin and Y. Wu, Mid-Infrared Nonlinear Optical Materials Based on Metal Chalcogenides: Structure–Property Relationship, *Cryst. Growth Des.*, 2017, **17**(4), 2254–2289.
128 K. Sayama, A. Nomura, Z. Zou, R. Abe, Y. Abe and H. Arakawa, Photoelectrochemical Decomposition of Water on Nanocrystalline BiVO 4 Film Electrodes under Visible Light, *Chem. Commun.*, 2003, 2908–2909.
129 S. R. Kavanagh, C. N. Savory, D. O. Scanlon and A. Walsh, Hidden Spontaneous Polarisation in the Chalcohalide Photovoltaic Absorber Sn2SbS2I3, *Mater. Horiz.*, 2021, **8**(10), 2709–2716.
130 X. Wang, Z. Li, S. R. Kavanagh, A. M. Ganose and A. Walsh, Lone Pair Driven Anisotropy in Antimony Chalcogenide Semiconductors, *Phys. Chem. Chem. Phys.*, 2022, **24**(12), 7195–7202.
131 K. M. Ok, Functional Layered Materials with Heavy Metal Lone Pair Cations, Pb^{2+}, Bi^{3+}, and Te^{4+}, *Chem. Commun.*, 2019, **55**(85), 12737–12748.
132 J. V. Handy, W. Zaheer, A. R. Rothfuss, C. R. McGranahan, G. Agbeworvi, J. L. Andrews, K. E. García-Pedraza, J. D. Ponis, J. R. Ayala and Y. Ding, Lone but Not Alone: Precise Positioning of Lone Pairs for the Design of Photocatalytic Architectures, *Chem. Mater.*, 2022, **34**(4), 1439–1458.
133 H. Suzuki, H. Kunioku, M. Higashi, O. Tomita, D. Kato, H. Kageyama and R. Abe, Lead Bismuth Oxyhalides PbBiO2X (X = Cl, Br) as Visible-Light-Responsive Photocatalysts for Water Oxidation: Role of Lone-Pair Electrons in Valence Band Engineering, *Chem. Mater.*, 2018, **30**(17), 5862–5869.
134 S. Al Bacha, S. Saitzek, H. Kabbour and E. E. McCabe, Iron Oxychalcogenides and Their Photocurrent Responses, *Inorg. Chem.*, 2024, **63**(7), 3292–3302, DOI: **10.1021/acs.inorgchem.3c03672**.
135 J. Cui, C. Li and F. Zhang, Development of Mixed-Anion Photocatalysts with Wide Visible-Light Absorption Bands for Solar Water Splitting, *ChemSusChem*, 2019, **12**(9), 1872–1888, DOI: **10.1002/cssc.201801829**.
136 H. Zhang, L. Liu and Z. Zhou, Towards Better Photocatalysts: First-Principles Studies of the Alloying Effects on the Photocatalytic Activities of Bismuth Oxyhalides under Visible Light, *Phys. Chem. Chem. Phys.*, 2012, **14**(3), 1286–1292.
137 J. Zhang, P. Zhou, J. Liu and J. Yu, New Understanding of the Difference of Photocatalytic Activity among Anatase, Rutile and Brookite TiO2, *Phys. Chem. Chem. Phys.*, 2014, **16**(38), 20382–20386.
138 J. Zhang, W. Yu, J. Liu and B. Liu, Illustration of High-Active Ag2CrO4 Photocatalyst from the First-Principle Calculation of Electronic Structures and Carrier Effective Mass, *Appl. Surf. Sci.*, 2015, **358**, 457–462.
139 J. Yang, P. Jiang, M. Yue, D. Yang, R. Cong, W. Gao and T. Yang, Bi2Ga4O9: An Undoped Single-Phase Photocatalyst for Overall Water Splitting under Visible Light, *J. Catal.*, 2017, **345**, 236–244.
140 Y. Yao, Q. Li, W. Chu, Y. Ding, L. Yan, Y. Gao, A. Neogi, A. Govorov, L. Zhou and Z. Wang, Exploration of the Origin of the Excellent Charge-Carrier Dynamics in Ruddlesden–Popper Oxysulfide Perovskite Y2Ti2O5S2, *Phys. Chem. Chem. Phys.*, 2023, **25**(48), 32875–32882, DOI: **10.1039/D3CP02860G**.
141 N. Vonrüti, *Ferroelectricity and Metastability in (Mixed-Anion) Perovskite Oxides for Improved Solar Water Splitting*, 2019.
142 S. Al Bacha, S. Saitzek, E. E. McCabe and H. Kabbour, Photocatalytic and Photocurrent Responses to Visible Light of the Lone-Pair-Based Oxysulfide Sr6Cd2Sb6S10O7, *Inorg. Chem.*, 2022, **61**(46), 18611–18621, DOI: **10.1021/acs.inorgchem.2c03040**.
143 N. Vonrüti and U. Aschauer, Catalysis on Oxidized Ferroelectric Surfaces—Epitaxially Strained LaTiO2N and BaTiO3 for Photocatalytic Water Splitting, *J. Chem. Phys.*, 2020, **152**(2), 024701.
144 R. F. Berger, C. J. Fennie and J. B. Neaton, Band Gap and Edge Engineering *via* Ferroic Distortion and Anisotropic Strain: The Case of SrTiO3, *Phys. Rev. Lett.*, 2011, **107**(14), 146804.
145 N. Vonrüti and U. Aschauer, Epitaxial Strain Dependence of Band Gaps in Perovskite Oxynitrides Compared to Perovskite Oxides, *Phys. Rev. Mater.*, 2018, **2**(10), 105401.
146 N. Vonrüti and U. Aschauer, Band-Gap Engineering in AB (O x S 1− x) 3 Perovskite Oxysulfides: A Route to Strongly Polar Materials for Photocatalytic Water Splitting, *J. Mater. Chem. A*, 2019, **7**(26), 15741–15748.
147 N. Vonrüti and U. Aschauer, Anion Order and Spontaneous Polarization in LaTiO 2 N Oxynitride Thin Films, *Phys. Rev. Lett.*, 2018, **120**(4), 046001.
148 J. Li, L. Cai, J. Shang, Y. Yu and L. Zhang, Giant Enhancement of Internal Electric Field Boosting Bulk Charge Separation for Photocatalysis, *Adv. Mater.*, 2016, **28**(21), 4059–4064.
149 S. Al Bacha, S. Saitzek, P. Roussel, M. Huvé, E. E. McCabe and H. Kabbour, Low Carrier Effective Masses in Photoactive Sr2Sb2O2Q3 (Q = S, Se): The Role of the Lone Pair, *Chem. Mater.*, 2023, **35**(22), 9528–9541, DOI: **10.1021/acs.chemmater.3c01298**.
150 F. Xu, Z. Li, R. Zhu, Y. Chu, Z. Pan, S. Xia, J. Fu, Z. Xiao, X. Ji, M. Liu and B. Weng, Narrow Band-Gapped Perovskite Oxysulfide for CO2 Photoreduction towards Ethane, *Appl. Catal., B*, 2022, **316**, 121615, DOI: **10.1016/j.apcatb.2022.121615**.
151 A. C. Hernandez Oendra, M. A. Aspect, J. L. Jaeggi, J. Baumann, C. R. Lightner, A. B. Pun and D. J. Norris, Tunable Synthesis of Metal–Organic Chalcogenide Semiconductor Nanocrystals, *Chem. Mater.*, 2023, **35**(21), 9390–9398, DOI: **10.1021/acs.chemmater.3c02275**.
152 N. Louvain, G. Frison, J. Dittmer, C. Legein and N. Mercier, Non-covalent Chalcogen Bonds and Disulfide Conformational Change in the Cystamine-Based Hybrid Perovskite [H3N(CH2)2SS(CH2)-2NH3]PbIII4, *Eur. J. Inorg. Chem.*, 2014, (2), 364–376, DOI: **10.1002/ejic.201301017**.
153 A. Kumar, D. W. Chang and J.-B. Baek, Current Status and Future of Organic–Inorganic Hybrid Perovskites for Photoelectrocatalysis Devices, *Energy Fuels*, 2023, **37**(23), 17782–17802, DOI: **10.1021/acs.energyfuels.3c02680**.
154 P. Mukherjee, K. Sathiyan, A. K. Vijay, R. Bar-Ziv and T. Zidki, Hybrid Nanostructure of Mixed Transition Metal Oxysulfides Supported by Porous PBA as Efficient Electrocatalysts for the Oxygen Evolution Reaction, *Isr. J. Chem.*, 2022, **62**(3–4), e202100110, DOI: **10.1002/ijch.202100110**.
155 A. L. Pacquette, H. Hagiwara, T. Ishihara and A. A. Gewirth, Fabrication of an Oxysulfide of Bismuth Bi2O2S and Its Photocatalytic Activity in a Bi2O2S/In2O3 Composite, *J. Photochem. Photobiol., A*, 2014, **277**, 27–36, DOI: **10.1016/j.jphotochem.2013.12.007**.
156 R. P. Tiwari, Visible-Light-Activated Enhanced Shift Current Bulk Photovoltaic Effect in Lead-Free Oxychalcogenide Perovskites: Emergence of Fully Inorganic Photovoltaic Materials, *J. Phys. Chem. C*, 2022, **126**(25), 10258–10265, DOI: **10.1021/acs.jpcc.2c01848**.